Novel Sagittal Bone Saw

Submitted By
Matthew P. Kelly

IN PARTIAL FULFILLMENT OF THE REQUIREMENTS FOR AN UNDERGRADUATE THESIS WITH A

BACHELOR OF SCIENCE IN MECHANICAL ENGINEERING

School of Engineering
Tufts University
Medford, Massachusetts

May 2011

Signature of Author:
Matthew P. Kelly

Certified By:
Associate Professor Thomas P. James
Department of Mechanical Engineering
Tufts University

Committee:
Anil Saigal
Department of Mechanical Engineering
Tufts University

Committee:
Dr. Eric Smith
Tufts University Medical Center

Abstract

A novel sagittal saw and fixture have been developed to test the hypothesis that a mechanically created impulsive thrust force can be used to increase the cutting rate in bone. Sagittal bone saws function through angular reciprocation, and are used primarily in applications that require plunge cutting of bone. Rapid cutting rate is important in orthopedic surgery because the patient is often under tourniquet, which puts a time limit on the surgery. It was proposed that an impulsive thrust force could be created by modifying the blade path to include a component of motion normal to the bone surface. A saw was designed and prototyped to test the effects of blade path on cutting rate in bovine cortical bone. At the start of each cutting stroke, the mechanism drove the blade into the surface of the bone, increasing the load applied to the surface with the intention to increase cutting rate. As each cutting stroke was completed, the blade was retracted from the surface, with the intention of clearing bone chips. Sagittal saws cut in two directions, so the pattern was repeated on the return stroke. The prototype saw was capable of reproducing both the pure arc motion found in typical sagittal saws and various figure eight motions. The forces driving the blade into and out of the bone acted against the inertia of the saw. The results of the experiments demonstrated that the addition of an impulsive thrust force produced a significant increase in cutting rate over pure sagittal arc motion.

Acknowledgements

I would first like to thank my thesis advisor, Professor Thomas James, for his directional guidance on all parts of this project. I am grateful for the opportunity he gave me to work on an excellent research project early in my academic career. I would also like to thank Dr. Eric Smith, of the Tufts Medical Center, who provided a practical understanding of the field of orthopaedics. I would like to show my gratitude to the Tufts Mechanical Engineering Department, and the Tufts Laboratory for Biomechanical Studies for funding this research.

A large part of this project was machine design, and the final result would not have been possible without the excellent guidance I received from the other members of the Biomechanical Lab. Professor Anil Saigal was especially helpful in guiding my design work so that the end result would be realistic and reliable. I would also like to show my gratitude to John Pearlman for his generosity and patience in helping me understand the machining process, as well as for his practical advice. I am grateful to James Hoffman for his excellent instruction in the machine shop, and assistance in the fabrication of the saw and fixture used in this thesis. I would also like to thank Vincent Miraglia and the Colby St. Machine shop for their help in the final stages of assembly and testing.

I would like to thank Timothy Lannin, for his help on all aspects of this project. In particular, he worked with me to on every experiment that was conducted, and helped me to understand and interpret the results. Finally, I would like to thank my parents, Karen and Peter Kelly, for their help in editing the thesis and for their continued support of my academic career.

Table of Contents

List of Tables

List of Figures

List of Appendices

List of Appendix Figures

1 Introduction

Orthopaedics is a branch of surgery that deals with the muscle and skeletal systems. An important tool used by orthopaedic surgeons is the sagittal bone saw. It is primarily used in situations where plunge cutting of bone is required, such as during hip and knee replacement. Sagittal saws are characterized by a long blade that oscillates symmetrically about its center, or sagittal, plane. A typical sagittal saw is shown in Figure 1.

FIGURE 1- Stryker Sagittal Saw

Sagittal saws have some serious drawbacks which can negatively affect patient outcomes. As the saw is cutting, a significant amount of heat is generated, which is transferred to the surrounding bone cells. It has been shown that if bone cells sustain a temperature of 44-47°C for longer than 1 minute then they can be damaged, and that cell necrosis can be caused by temperatures above 61°C (1). In a typical surgery temperatures can reach 200°C, routinely damaging or destroying a large number of cells in the immediate area of the cut (1). This damage to bone cells can delay patient recovery time and can make the surgery less effective if it leads to infection and implant misalignment (2) (3).

Cutting rates of sagittal saws are dependent on bone type and density. Higher density cortical bone is more difficult to cut than lower density cancellous bone. Bone density also varies from patient to patient. In cases where the cutting rate is low, the duration of the cut becomes a concern. Time is limited during many orthopaedic surgeries, especially those that make use of a tourniquet, such as total knee arthroplasty (4). The pressure of time motivates surgeons to increase cutting rates, which is typically done by applying a higher thrust load. Although this method is functional, it reduces surgeon control and increases the chance that the saw could break through the back of the bone causing unnecessary damage to surrounding tissue.

Statement of Hypothesis:

It was hypothesized that the application of an impulsive thrust load to the saw blade during cutting would produce a higher cutting rate when compared to a conventional sagittal saw.

A novel sawing mechanism was developed to test this hypothesis. The impulsive loading was created in a method similar to a jackhammer. A small mass that is rapidly changing direction uses the inertia of a larger mass to generate loads which are greater than those applied nominally to the large mass. This effect is synchronized with the motion of the blade such that the mechanism provides a large force at the start of each stroke, and then retracts the blade near the end of each stroke. The motion of the blade was symmetric on the return stroke, cutting equally in each direction and balancing forces at the blade tip. In addition to increasing the effective thrust load at the start of the cut, this mechanism likely reduces the frictional loading and aids in chip clearance near the end of the cut.

A test fixture was designed and built to enable scientific testing of the novel sawing mechanism. The fixture was used to guide the saw on a repeatable path through the bone, which was clamped

in an adjustable vice. The fixture maintained a constant applied force throughout the cut, which was adjusted before each experiment. A design of experiments was performed to determine the effect of each mechanism parameter on cutting rate.

Research Objectives:

1) Identify sawing parameters which are relevant to cutting rate

2) Design and build a novel sawing mechanism to validate hypothesis

3) Design and build a research fixture to carry out experiments

4) Conduct experiments to determine if an impulsive thrust force improved cutting rates

2 Background

Motivation for Study:

Orthopaedic surgery has become commonplace in society with numerous surgeries each year, many of which involve bone sawing. Evidence suggests that bone saws for amputation have been a part of society for at least two millennia (5). Although modern saws are sharper, powered at high speeds, and sterile, their basic method of operation is strikingly similar to that of their predecessors. Despite these advances, there are still situations where the cutting rates of modern saws are insufficient. Postoperative results are affected by the quality of a cut in orthopaedic surgery (6), suggesting that a better bone saw would be able to benefit patients.

Although there has been a large amount of research conducted on sawing, the majority of experiments have been done on metal or wood. The information obtained through metal sawing research does not necessarily translate to bone sawing because of the anisotropic and heterogeneous nature of bone. Bone is comprised of a large number of roughly cylindrical structures known as osteons, or haversian systems. There are roughly 1,500 osteons per square centimeter in adult human bone, with each having a diameter on the order of 200μm (5). These structures affect the crack formation and propagation in bone, and are large enough that they cannot be neglected when considering the mechanics of bone sawing. Previous research in bone sawing has provided insight into how the structure of bone is involved in the sawing process, and what sawing parameters have the most effect on cutting rates.

Literature Survey

Bone sawing is challenging to study because of the complex structure and organic nature of bone. Orthogonal machining is one method of simplifying both the modeling and experimental aspects of bone sawing. Many researchers (5) (6) (7) (8) (9) have utilized this experimental method, also known as Merchant analysis. This special type of machining analysis was developed by Ernst (10) and Merchant (11) in the 1940's to understand how chips were formed in the machining of metals. Orthogonal machining reduces the three-dimensional case of standard machining to a planar case by assuming that the tool is wider than the work piece, thus eliminating edge effects. Additionally, a single tooth is used to cut what is assumed to be a continuous chip. The radius of the cutting edge is generally considered to be of negligible size when compared to the depth of cut. Finally, the tool moves in a direction orthogonal to the cutting edge. These conditions can be readily created in a lab, and thus facilitate the development and validation of a variety of simple models relating cutting parameters to cutting rate, energy, and temperature.

Although researchers would prefer to conduct experiments on human bone, this is logistically impractical. Instead, many researchers carry out their tests using bovine bone, which has been shown to produce similar results when compared to human bone. The mechanical properties of bone can be preserved by storing in a saline solution, and freezing until ready for use. Prior to conducting experiments, bones are typically stored in a refrigerator and allowed to thaw while fully immersed in saline solution. This protocol helps to preserve the structure of the bone for a prolonged period of time (5) (8).

One common parameter to study is the specific force of cutting as a function of depth of cut (DOC). In general, the force per cutting edge width increases with DOC as shown in Eqn. 1 (7). At zero DOC the force does not drop to zero. This is because the bone under the tooth is deflecting slightly instead of being cut, creating a frictional load.

F $Cutting\ force\ per\ width$
F_0 $Frictional\ load\ per\ width$
K $Experimental\ Constant$
t $Dimensionless\ DOC$
n $Size\ effect,\quad 0 < n < 1$

$$F = K \cdot t^n + F_0 \qquad Eqn.\ 1$$

Although cutting forces are important, it is often more useful to know how much energy is required to remove a volume of bone. For constant power, reducing the specific cutting energy will increase the cutting rate. The volumetric specific energy for sawing was found to decrease with an increasing DOC (5) (7) (9). This is because the volume removed increases linearly with depth, but the force increases by a fractional power. Alternatively, the energy of formation is related to the surface area to volume ratio of the chips, and a larger DOC yields a smaller ratio. These findings suggest that, for a constant power output, increasing the DOC will increase the cutting rate.

Cutting speed is another parameter that has been shown to have an influence on the forces involved in bone sawing. Kraus (8) demonstrated that both the cutting and thrust forces increased with cutting speed up to a critical speed, after which there was a large reduction in forces. It is suggested that this was due to the existence of a critical crack formation velocity in bone, and that the critical feed rate is roughly 50mm/s. The difference in force was hypothesized to be a result of a transition from controlled crack propagation around osteons to catastrophic crack

propagation directly through osteons. Thus, blade speed is important in sawing because it is related to crack initiation and therefore chip formation.

In addition to blade speed, chip formation is strongly affected by the DOC. Plaskos (7) demonstrated that the chips formed at small DOC (2μm) are nearly continuous and curl off the tool with a significant degree of plastic deformation, resembling chips formed by metal machining. For large depths of cut (200μm) chips are formed through discrete fracture, and subsurface damage was found to be dramatically increased over the small DOC trials. For the large depths of cut the forces were observed to fluctuate, further supporting the fracture formation theory. Both of these trials were carried out at 3500mm/s, a speed which is representative of those found in a typical orthopaedic procedure with sagittal saws. (3)

Further work on crack formation was carried out by Wiggins (5) and Krause (8). Wiggins conducted experiments at 8.5mm/s and a DOC of 254μm, and noted that chips tended to form through discrete fractures and were not plastically deformed. It was also noted that fractures did not readily propagate across osteons. Krause conducted a similar study (speed = 1.27-25.4mm/s, DOC=70μm) and confirmed that chips were formed through discrete fractures, noting that cracks propagated in front of the tool. The experiments conducted by Wiggins and Krause both show that, for large DOC and small blade speeds, chips are formed through discrete fracture and that cracks propagate around osteons.

The research of Wiggins and Kraus showed that bone chips are formed through fracture, suggesting that bone sawing may be similar to cutting through a brittle material such as concrete.

Jackhammers and rock drills are two examples of machines which have been developed specifically for breaking through brittle materials. These tools use a percussive action to break through hard brittle materials. These tools are effective because they create a large impulsive thrust force that initiates cracks more effectively than a smaller static thrust force. Thus, if bone chips are created through fracture, it would follow that a mechanism which creates an impulsive thrust force would be able to improve the cutting rate in bone. Krause (8) tested a similar concept by conducting an experiment in which a lateral vibration was applied to the tooth during cutting. It was found that this vibration dramatically reduced the force and energy required to cut bone.

In wood and metal sawing, it has been shown that an effective way to increase the cutting rate of a saw is to modify the blade path to increase the thrust loading. In 1959, Papworth (12) proposed a mechanism for creating a reciprocating saw with an oval stroke, thus imparting a component of blade motion normal to the work piece. It was proposed that this mechanism helped clear chips from the blade, thus improving sawing action. Further improvements were made in jig saws and reciprocating saws by several companies including Black & Decker (13) and the Milwaukee Electric Tool Corp. (14). The patents for these tools emphasized the effectiveness of these modifications at increasing cutting rate in wood, metal, and plastic. The success of these construction tools suggest that a similar principle may be successfully applied to surgical tools used for bone sawing.

Conclusions Based on Literature Study:

A primary focus of research on bone sawing has been the use of single cutting edge orthogonal machining to study the effects of DOC and cutting speed on cutting energy and forces. Few studies on bone sawing have been conducted at the oscillating speed of a sagittal saw and related

DOC using a multi-cutting edge saw blade. Furthermore, there have been no studies investigating the idea of impulsively loading the blade during cutting.

One of the primary differences between orthogonal machining and the operation of a bone saw is the DOC. In orthogonal machining analysis, the DOC is preset by the research fixture, and is generally limited by the capabilities of the fixture. In a bone saw, the DOC is a dependent variable, and can be arbitrarily small when compared to the cutting edge radius. In addition to DOC, orthogonal machining ignores the need for chip clearance, and the effects of multiple teeth.

Although impulsive loading of the blade has been shown to be effective in wood and metal cutting (12) (13) (14), it has not yet been tested on bone. Krause (8) showed that lateral vibrations of the blade are effective in orthogonal machining of bone, suggesting that impulsive loading of a saw blade would also be effective in bone.

Previous research shows a larger DOC results in larger forces and more efficient cutting (5) (7) (9). This suggests that an increase in thrust force will yield a larger DOC and more efficient cutting. If a saw is running at constant power, more efficient cutting translates to a higher cutting rate, which is preferred by surgeons. In the operating room, a surgeon can only apply a limited thrust load to the saw before reducing his or her ability to control the saw. It was proposed that a mechanism could be used to impart an impulsive thrust force on the blade during the cutting stroke. This mechanically applied thrust force would be far larger than the surgeon could apply, thereby increasing cutting rates while maintaining the control of the surgeon.

Mechanism Design:

A research saw mechanism was designed to test the effect on cutting rate of impulsively loading the bone surface during sawing. In order to achieve this goal, the saw was designed to cut both with and without the impulsive loading. Additionally, the saw provided the user with the ability to adjust the stroke length, blade speed, and applied static load.

Impulsive loading can be created by modifying the blade path to include a component of motion normal to the bone surface. This concept is already used with great success in commercially available wood saws, which cut through linear reciprocation. Each tooth on a reciprocating saw follows a quasi-elliptical orbit, creating a cutting force which is always in the same direction. While this is effective in linear reciprocating saws and jigsaws, it causes a loss of control in a sagittal saw. This is because in a linear saw the cutting force is directed along the length of the blade into the handle, where as in a sagittal saw, the cutting force is directed perpendicular to the length of the blade, creating a net moment on the handle. This difficulty can be overcome by creating a blade path shaped like a figure-eight, which alternates the direction of the cutting force. This creates an average moment on the handle of zero, which allows the saw to be controlled. Mathematically, a figure-eight blade path is defined by a parametric equation of the form shown in Eqn. 2.

$$R(t) = \langle Sin(t), Cos(2t) \rangle \qquad Eqn.\ 2$$

Physically, Eqn. 2 describes two oscillations which are occurring normal to each other, with one being twice the frequency of the other. In a machine, a 2:1 gear set can be used to create the correct frequency and phase of the two motions. An oscillating linear motion can be created through a rotational to linear converter. A typical rotational-to-linear converter is the slider-crank

mechanism, a simplified model of which is shown below in Figure 2. The crankshaft rotates about its center and the slider moves back and forth in the direction shown.

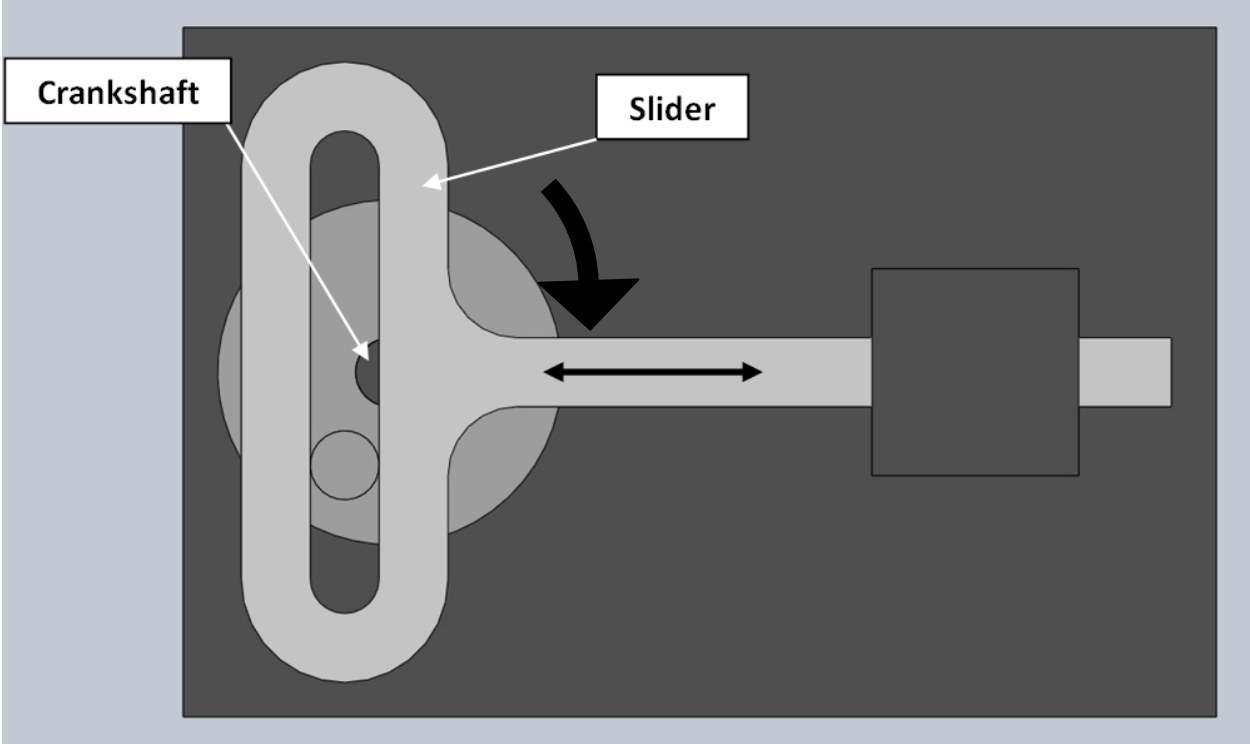

FIGURE 2- Slider Crank Mechanism

The mechanism used in this research was based on two slider-crank mechanisms, each driven from their own crankshaft. The two crankshafts were linked by a 2:1 gear-set. This arrangement produced a figure-eight path similar to that shown in Figure 3. In this paper, cutting and thrust amplitude refer to the distance from the center of the figure-eight blade path to the maximum value along a specific axis. Stroke length refers to the difference between the maximum and minimum values along a given axis. Along a given axis, the stroke length is twice the amplitude. The thrust and cutting amplitude of the path can be independently adjusted to create a wide variety of figure-eight paths. It should be noted that the path shown in Figure 3 is that of a tooth at the center of the blade. The teeth located away from the blade center followed slightly different blade paths because of the geometry involved, and are further discussed in Appendix A.

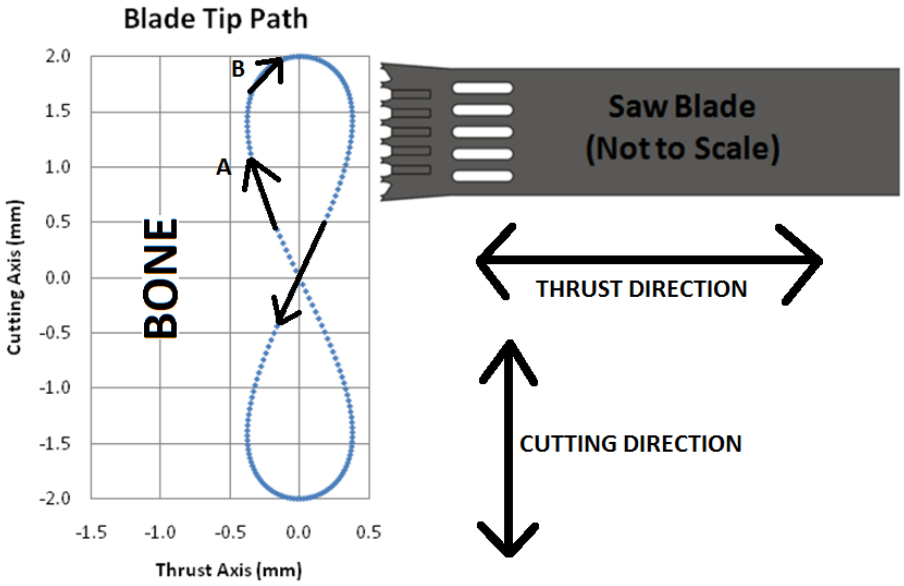

FIGURE 3- Figure Eight Path

In addition to thrust and cutting amplitude, the overall form of the blade path shape was adjusted by changing the phase angle of the gearing. Phase offset refers to a difference in the angle that the off-center crank on each shaft has when the gears are meshed. This enabled the experimenter to have more control over the locations and angles at which the blade strikes the bone. Figure 4 shows the effect of the phase offset of the gearing. A kinematic analysis of blade path is shown in Appendix A.

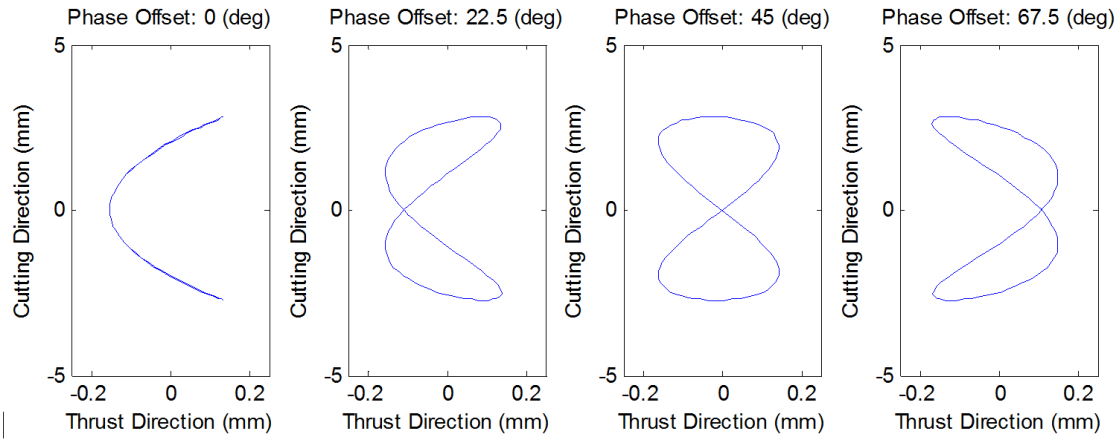

FIGURE 4- Phase Effects on Blade Path

3 Design of Experimental Apparatus

The goal of this research project was to determine the effect on cutting rate of an impulsive thrust force. In order to conduct these experiments, it was necessary to design a custom research saw and fixture.

Research Saw and Fixture Design Constraints:

Saw:

- The mechanism must move the blade such that it creates a balanced moment about the blade pivot axis
- The cutting amplitude should be variable from 0 to 3.0mm (0.12in)
- The thrust amplitude should be variable from 0 to 0.2mm (0.03in)
- Mechanism tolerance controlled such that blade path can be accurate to ±0.05mm (0.002in)
- Cutting frequency variable from 0 to 200Hz (12,000 oscillations per minute)
- Maintain blade oscillation frequency to within 1% of desired frequency
- Ability to adjust phase offset to within 5°
- Withstand normal operating loads without mechanism damage

Fixture

- Fixture must guide saw through a repeatable path
- Fixture must provide constant (±0.2N) force throughout cut
- Constant applied force must be adjustable from 0 to 80N (18lbf)
- Fixture must provide means of locating and restraining bone during experiments

Off-Center Crank Design

The central components in the sawing mechanism were two off-center crank mechanisms. While it is relatively simple to create these mechanisms using sliding contacts, this was not feasible due to the high speeds and precision required for the research device. Rotary ball bearings were used to secure all contact points on the crankshafts, including the off-center crank. The sliding components were connected using ball bearing linear guides. Figure 5 shows a cross section of one of the off-center crankshaft assemblies, which transmitted power from the gear to the carriage of the linear guide.

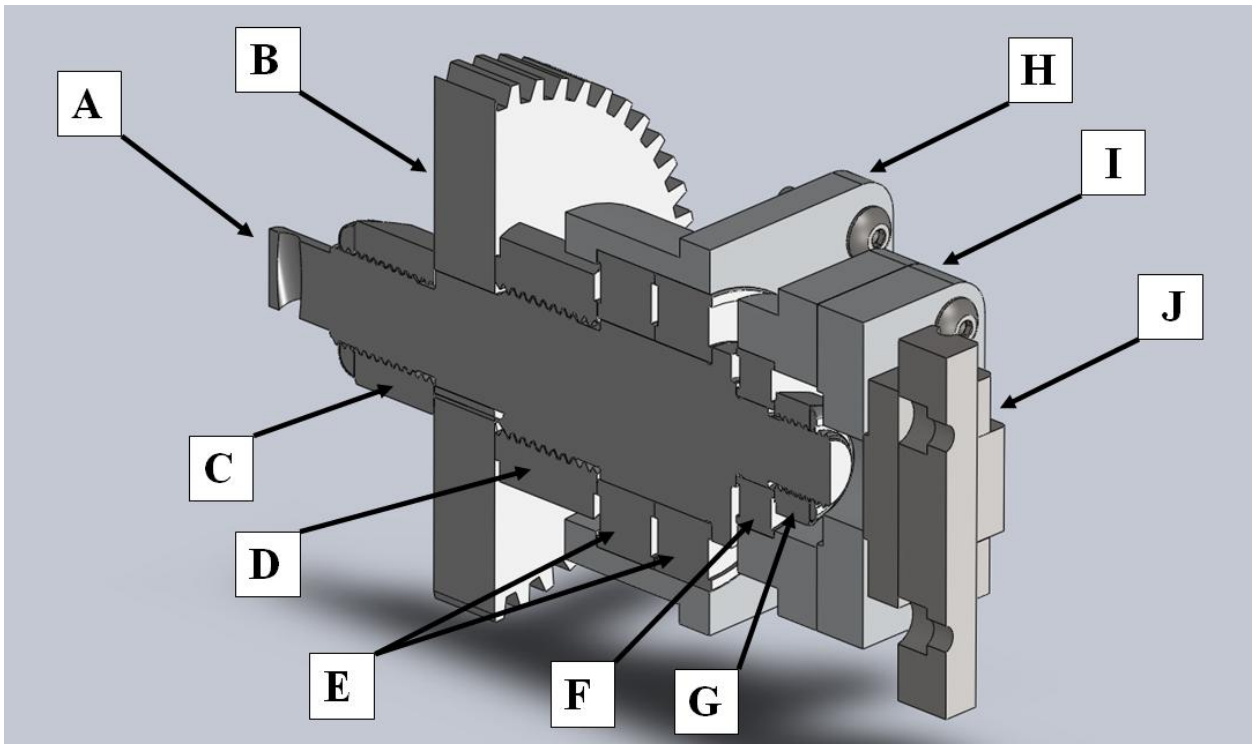

FIGURE 5- Off-Center Crank Assembly

A: **Cutting Crankshaft:** Transmits power from the gear to the linear guide
B: **Drive Gear:** Driven by the motor pinion on the main drive shaft, this gear powers the crank shaft
C: **Modified Lock-nut:** Keeps the gear from slipping off the shaft
D: **Modified Nut:** Keeps the crankshaft from sliding out of the support bearings
E: **Large Bearings:** Press-fit into the housing, slip-fit onto crankshaft
F: **Small Bearing:** Press-fit into the housing, slip-fit onto crankshaft
G: **Small Modified Nut:** Holds small bearing and housing onto the crankshaft
H: **Large Bearing Housing:** Supports large bearings, and is bolted to base plate
I: **Small bearing housing and plate:** Provides means of attaching linear guide
J: **Linear Guide:** Isolates a component of motion from the off-center crank

Mechanism Design:

Figure 6 shows several key components required to generate the "figure-eight" blade path. In order to achieve a sagittal cutting motion, it was necessary to constrain the centerline of the blade. This was done by attaching a rotational and linear bearing between the fixed shaft and blade holder. By constraining the centerline of the blade, the linear motion produced by the cutting crankshaft was converted to an angular rotation of the blade holder. The fixed shaft and

cutting crankshaft constrained the blade in the cutting direction, but left it free to slide in the thrust direction. This last degree of freedom was controlled by the thrust crankshaft.

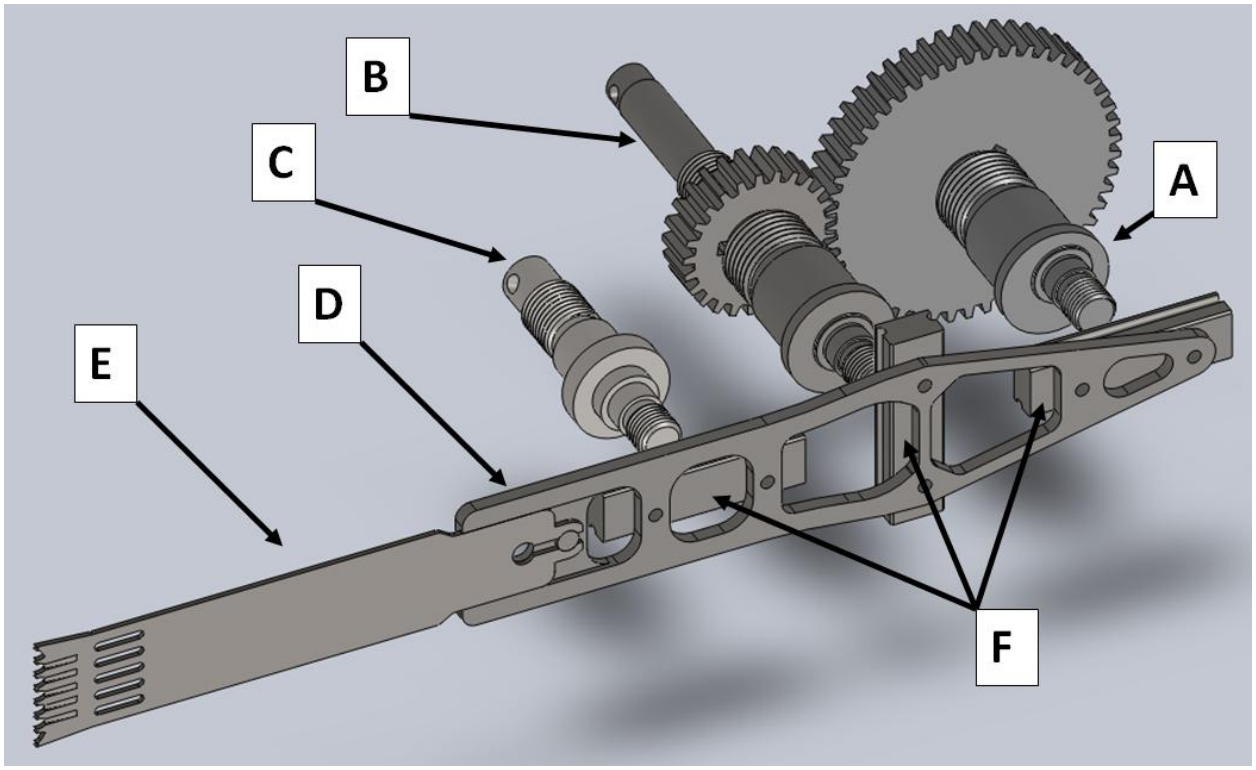

FIGURE 6- Selected Mechanism Components

A: Cutting Crankshaft
B: Thrust Crankshaft
C: Fixed Shaft
D: Blade Holder
E: Blade
F: Linear Guides

Motor Considerations:

A 2¼ horsepower router motor (Porter Cable, Model 892, Jackson, TN) was selected for the saw because it was capable of providing the loaded power and speed necessary for the saw. The motor came with a stock speed control module which did not enable the router to be run at low speeds. This module was removed, and replaced with an external variable AC power supply (Staco, Model SPN1510B, Staco Energy Products Co., Dayton, OH) which provided a greater

degree of accuracy in speed over the entire range from 0-22,000 Hz. The motor of the router was removed from its stock housing, and a custom housing was designed to hold it more securely. This housing enabled the motor output shaft to be precisely aligned with the saw driveshaft. The motor was connected using a high speed coupling. The saw and motor were both mounted to a large base plate and a polycarbonate guard was designed to enclose the moving parts. Figure 7 shows the saw, motor, and guard assembly.

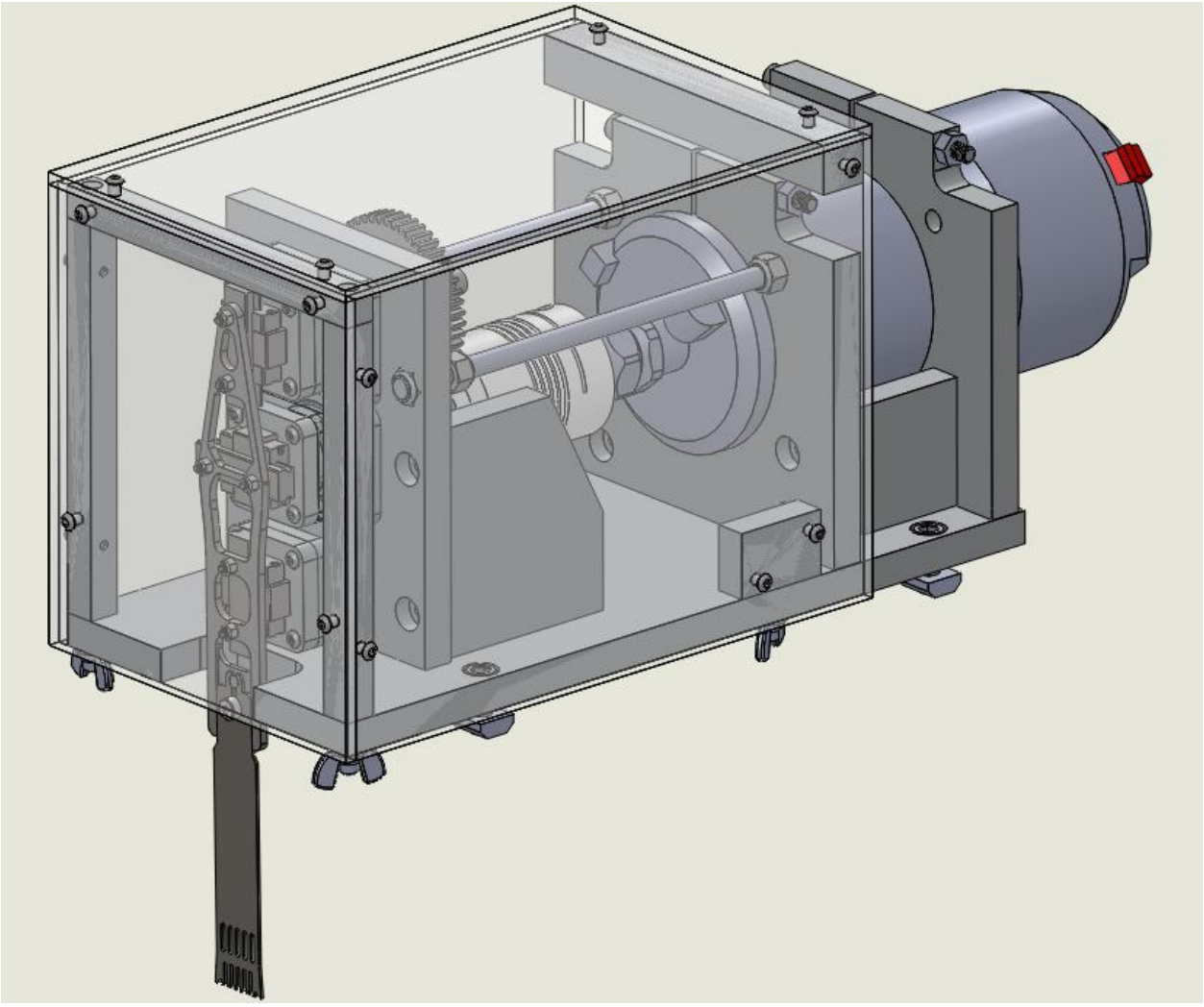

FIGURE 7-Saw, Guard, and Motor Assembly

Fixture Design:

In order to perform repeatable experiments, it was necessary to mechanically guide the saw through each cut at a prescribed constant force. This was accomplished by mounting the saw on a rotating frame with a counter-mass as shown in Figure 8.

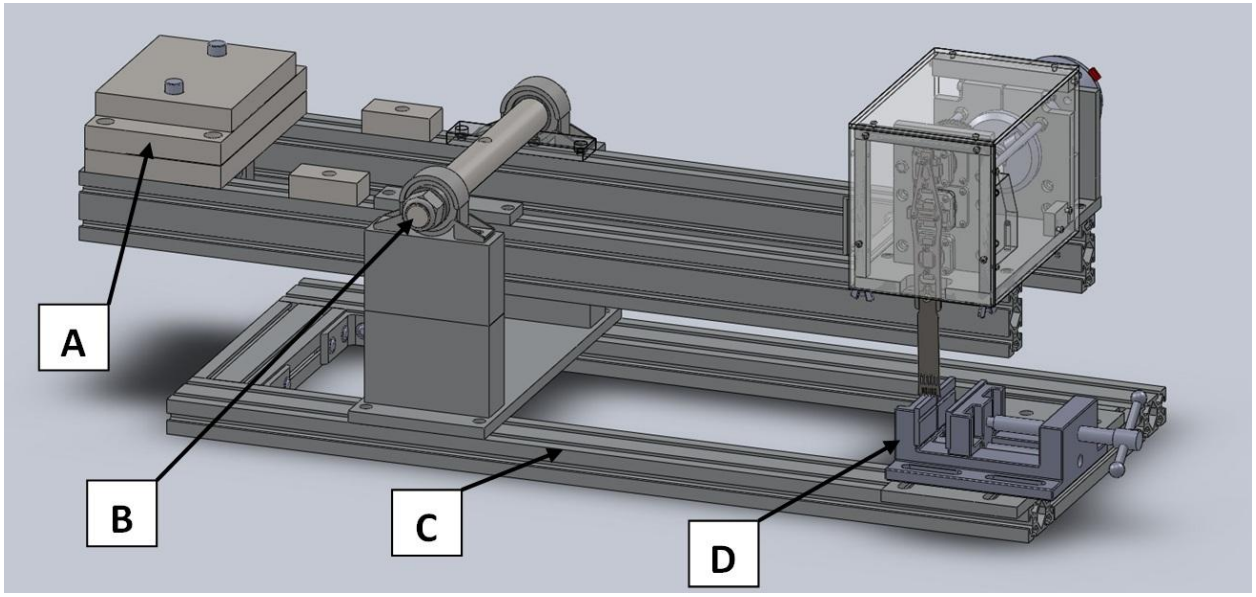

FIGURE 8- Experimental Fixture

A: Counter-mass
B: Main axle
C: Adjustable Base
D: Machine Vice

The main axle and counter-mass were moved along the rigid beam to change the force that was applied at the center tip of the saw blade. Ball bearings located on the main axle provided for a low friction pivot and repeatable rotation. As the saw cut through the bone, it caused the entire assembly to rotate. This rotation created a slight variation in the force applied at the tip of the blade. The force variation was measured to be 0.1N (0.02lbf), which is negligible when compared to the error in the force measuring device (MG20, Mark 10 Co., Copiague, NY) used (±0.4N). See Appendix B for a detailed analysis of the change in applied force as a function of rotation angle.

The structure of the fixture was primarily constructed with an aluminum extrusion (80/20 Inc., Columbia City, IN) which enabled the sliding adjustment of the pivot axle and counter mass. A standard machine vice (Palmgren 12403 DPL40 Low-Profile Vice, Chicago, Illinois) was used to hold the bone throughout the experiment.

Design for Fabrication:

In designing the fixture, it was necessary to consider the methods by which each component was produced, and how this affected the overall design objectives. The majority of the custom parts in the research saw and fixture were designed to be easily made using manual lathes and milling machines in the Tufts machine shop. In many cases, parts were designed to match stock material sizes to reduce machining time. The only parts which were made using CNC machines were those parts which would have been impractical to machine manually such as the blade base and the router clamping plates. All parts were machined by the designer, under the guidance of machine shop staff.

Material Selection:

There were several important considerations involved in the material selection for saw components. Since the saw was cutting bone, efforts were taken to use materials which would be resistant to corrosion. Many parts in the saw were moving at high speeds, so strength and safety were also important. The majority of the structure of the saw was machined from half inch aluminum plate. This was convenient because the material could be purchased in bulk, and the parts were designed to be a half inch thick to reduce machining time. For components under static and dynamic loading, materials with an appropriate modulus and geometric moment of

inertia were considered in the design. Table 1 provides a summary of the primary materials used in the saw and research fixture.

Table 1- Material Selection

Material:	Components:	Relevant Features:
aluminum 6061 plate:	saw structure, router housing, fixture mounting plates, frame for polycarbonate guard	corrosion resistance, low cost, easy to machine, high strength to weight ratio
aluminum 6061 bar:	bearing housings, fixture riser blocks	
80-20 aluminum extrusion	all structural components of fixture	ease of manufacture, low deflection, adjustability
steel alloy 1144 rod:	crankshafts	higher strength steel, easy to machine, low distortion after machining
stainless steel 304 plate:	blade holder	corrosion resistance, high hardness (good wear properties), able to be machined
stainless steel 440C:	linear bearings	mild corrosion resistance, excellent wear resistance, high strength
polycarbonate plate:	safety guard	transparent to light, high impact resistance
low carbon steel	browning change gears	higher strength and speed rating than nylon gears
zinc plated or SS-18:	fasteners	corrosion resistance, strength
aluminum / stainless steel:	high speed coupling	stainless steel bellows for fatigue and corrosion resistance, aluminum coupler for low weight

4 Experimental Methodology

The experimental goal was to determine the effect that a variety of sawing parameters had on volumetric cutting rates for bone sawing. The fixture and saw design provided for a variety of independent parameters to be controlled. In these experiments, cutting rate was determined as a function of saw speed, thrust amplitude, and static load. Several parameters were held constant, including stroke length, phase offset, and sample cross section. Temperature measurements were considered to be outside the scope of this project, and will be considered by future researchers.

Bone Sample Preparation:

Sections of bovine bone were purchased from an approved abattoir[1], and frozen at -10 °C (14°F) for storage. The bone sections were taken from mid-diaphysis of the femur of adult cows, ages 2-3 years. In preparation for the experiments, samples were cut from the frozen bones. The cancellous bone and marrow were then removed, leaving behind the cortical bone. Bone samples were machined to a cross section of 19.8mm (0.78in) by 5.60mm (0.22in) and a length of 75mm (3.0in). The length dimension was parallel to the primary osteon direction of the bone sample. Bone samples were then immersed in Hank's Balanced Salt Solution (reference number 14065-056) and stored at 5.6°C (42°F) until ready for use. The bone sections were temporarily removed from the solution for cutting and returned after each cut. For each data point, a cut was made from each of three different bone samples to control for differences across the samples. The same three samples were used for all cuts in the experiment. Successive cuts on each bone were made with a minimum spacing of 3.0mm (0.12in) to reduce edge effects. Bones were an average

[1] Blood Farms, 94 West Main Street, Groton, Massachusetts 01450

density of 2100kg/m^3. The mass of each sample was determined using triple beam balance, and the volume was determined by immersion in a graduated cylinder. Density was calculated from these measurements. Table 3 provides a summary of the bone sample properties.

Table 2- Bone Sample Properties

Bone Sample Statistics	**Width (mm)**	**Height (mm)**	**Bone Density (kg/m^3)**
Average	19.8	5.6	2097
Standard Deviation	0.4	0.2	151

Load and Speed Calibration, Bone Clamping:

Before the start of each experiment, the research saw was configured to produce the correct blade path, including cutting stroke length, thrust amplitude, and phase offset. The cutting stroke length and thrust amplitude were determined by the geometry of the off-center crankshafts, which were measured using a dial indicator and lathe prior to assembly. The phase offset was adjusted in discrete increments through re-meshing of the gear teeth. The pivot axle position for the fixture was adjusted to provide the desired nominal thrust force. This thrust force was measured at the tip of the saw tooth, in the middle of the saw blade, using a portable force gage (MG20, Mark 10 Co., Copiague, NY) with an accuracy of ±0.4N. The sawing frequency was precisely controlled using a 120V, 15Amp variable transformer (Staco, Model SPN1510B, Staco Energy Products Co., Dayton, OH). The shaft speed of the sawing mechanism was measured using a handheld tachometer (Checkline A2108, Electromatic Equipment Co., Cedarhurst, NY) with a precision of ±1 Hz during sawing. The RMS speed of the blade tip was calculated numerically using LabVIEW. The geometry of the mechanism and instantaneous blade speed were used to plot the blade path as a function of time, as shown in Eqn. 3. The RMS speed was then determined using Eqn. 4.

T $cycle\ period$
t $time\ since\ cycle\ start$
$x(t)$ $position\ of\ blade\ tip\ along\ thrust\ axis$
$y(t)$ $position\ of\ blade\ tip\ along\ cutting\ axis$
$P_0(x,y)$ $position\ vector\ of\ the\ blade\ tip, see\ Appendix\ A$

$$P_0 = \langle x(t), y(t) \rangle \qquad Eqn.\ 3$$

$$RMS_{Speed} = \sqrt{\frac{1}{T}\int_0^T \left[\left(\frac{dx}{dt}\right)^2 + \left(\frac{dy}{dt}\right)^2\right] dt} \qquad Eqn.\ 4$$

At the start of each test, a sample was clamped into the vice, and positioned beneath the center of the blade as seen in Figure 9. The bone was supported from below using machining parallels. At the start of each cut, the saw was allowed to reach the desired speed before the blade was slowly lowered into contact with the sample. A LabVIEW VI was used to measure the duration of the cut from the instant the blade contacted the bone to the time that the cut was completed. For each set of sawing parameters, three trial runs were performed.

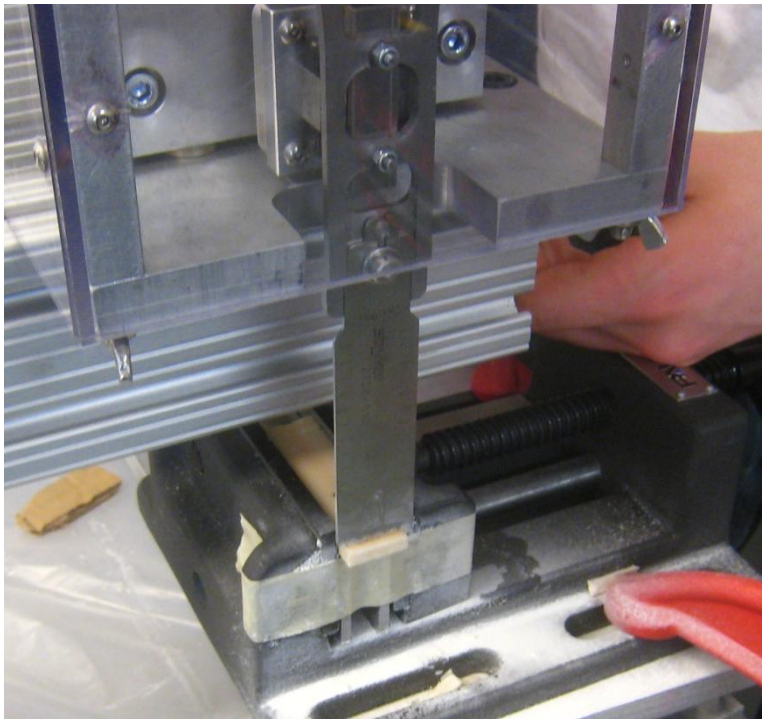

FIGURE 9- Bone Clamping Set-up

Design of Experiments:

The first study to be conducted for this research was to determine the effect of oscillating blade speed on cutting rate. Speed has been shown to be an important variable in chip formation and crack propagation (8), and thus it follows that cutting rate would be dependent on speed. Modern sagittal saws have the ability to cut at a variety of speeds (3) further suggesting that speed is an important parameter. The applied load for this first study was determined by trial and error, starting with 4.9N (1.1lbf) (1). An acceptable loading was found to be 7.6N (1.7lbf). Speeds were selected by starting with the lowest speed that provided an appreciable cutting rate, and then increasing speed over successive trials towards the upper limits of the saw. The higher oscillating blade speeds are similar to those found in commercial sagittal saws (3).Table 3 provides a summary of the values for parameters used in this first study.

Table 3- Parameters for Cutting Rate vs.. Blade Speed 1

Cutting Rate vs. Blade Speed 1		
RMS Cutting Speeds:	96 Hz	706mm/s (1670in/min)
	113 Hz	829mm/s (1960in/min)
	129 Hz	952mm/s (2250in/min)
	146 Hz	1080mm/s (2550in/min)
Constant Parameters		
Stroke Length:	3.38mm (0.133in)	
Sample Width x Height	9mm (0.4in) x 10mm (0.4in)	
Blade:	Stryker Dual Cut 4125-135-090	
Static Load:	7.6N (1.7lbf)	

In the first speed study, the cross sectional area of the bone was calculated from digital images of the bone samples after each cut. The image processing algorithm was developed using ImageJ software, an open source Java code from the US National Institute of Health website (http://rsbweb@nih.gov.ij/). For all other studies, the samples were milled to rectangular cross section so that the cross sectional area could be calculated from the width and height of the sample.

A second speed study was conducted with a different blade and sample geometry to address some problems which came up in the first trial. The new blade was selected for a variety of reasons, most importantly its closer tooth spacing. The samples that were used in the second speed study also had a wider cross-section. A detailed discussion of these differences can be found in the following Results and Discussion section. The speeds were selected to be similar to those used in the first speed study, and the load was adjusted to provide a similar force per tooth. Table 4 summarizes the values of the experimental parameters used in the second speed study, and Table 5 provides details on the differences between the blades used in each experiment.

Table 4- Parameters for Cutting Rate vs.. Blade Speed 2

Cutting Rate vs. Blade Speed 2		
RMS Cutting Speeds:	117 Hz	541mm/s (1280in/min)
	133 Hz	617mm/s (1460in/min)
	142 Hz	658mm/s (1550in/min)
	160 Hz	741mm/s (1750in/min)
Constant Parameters		
Stroke Length:	2.37mm (0.093in)	
Sample Width x Height	19.8mm x 5.6mm (0.78in x 0.22in)	
Blade:	Stryker 2108-110	
Static Load:	14.4N (3.24lbf)	

Table 5- Comparison of Blades

	Speed Study 1 **Stryker Dual Cut 4125-135-090**	**Speed Study 2** **Stryker 2108-110**
Tooth Spacing	3.43mm (0.135in)	2.12mm (0.083in)
Set (single tooth)	none	0.12mm (0.005in)
Thickness	1.14mm (0.045in)	1.22mm (0.048in)
Width	25.0mm (0.984in)	24.8mm (0.978in)
Length	108.9mm (4.288in)	86.7mm (3.415in)
Rake Angle	10°	-30°, symmetric tooth
End Curvature	None- Straight Blade	Radius 86.7mm (3.415in)

The final study was a full factorial to determine cutting rate as a function of static load, thrust amplitude, and oscillating blade speed. The values for the parameters in this study were determined from screening experiments. The Stryker 2108-110 blade was used because of its superior performance to the Dual-Cut blade in the cutting rate vs.. blade speed trials. The thrust amplitude was selected to be as small as tolerances allowed. This decision was made based on an earlier test where a large thrust amplitude of 0.5mm (0.02in) was used, and the motion was too aggressive to be effective. Table 6 summarizes the values for the independent and dependant parameters used in the full factorial study.

Table 6- Parameters for Full Factorial Study

Independent Parameters- Full Factorial		
Applied Static Load:	14.4N (3.24lbf)	19.4N (4.36lbf)
RMS Blade Speed:	660mm/s (1560in/min)	741mm/s (1750in/min)
Thrust Amplitude:	0mm (0in)	0.05mm (0.002in)
Constant Parameters- Full Factorial		
Stroke Length:	2.37mm (0.093in)	
Sample Width x Height	19.8mm x 5.6mm (0.78in x 0.22in)	
Blade:	Stryker 2108-110	
Phase Offset:	65° (1.13rad)	

5 Results and Discussion

Three experiments were conducted as part of this research. The first two studies considered cutting rate as a function of blade speed, and the final study considered cutting rate as a function of blade speed, static load, and thrust amplitude.

Cutting Rate vs.. Oscillating Blade Studies:

The first experiment was performed to determine the effect of blade speed on cutting rate for a thrust amplitude of zero (conventional sagittal sawing configuration). For low blade speeds, a relatively small and constant cutting rate was observed. The cutting rate increased rapidly for tip speeds greater than 800mm/s. Figure 10 shows the results for volumetric cutting rate as a function of blade speed in the first trial.

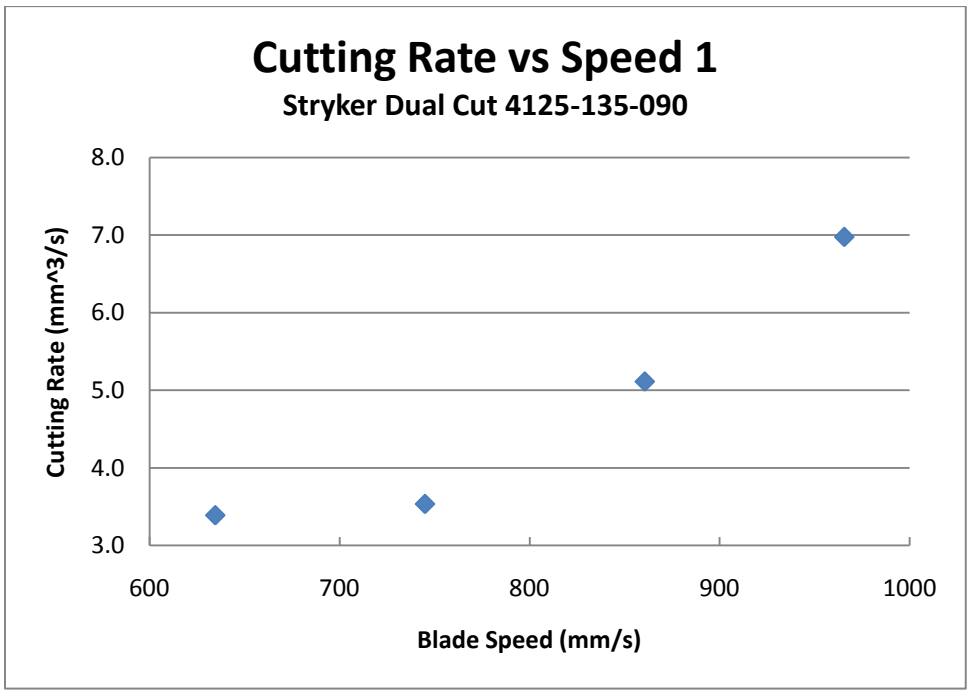

FIGURE 10- Cutting Rate vs.. Speed 1

This first speed study was carried out on bone samples with an approximate width of 9mm. The saw blade was approximately 25mm long, which meant that only a small portion of the blade was being used. In surgery, it is likely that the entire cutting edge of the blade would be engaged, so a second speed study was conducted which used a wider sample (20mm). In the first speed study, bone samples were cut to approximately the same size, but the width of the samples was not rigorously controlled. In this case, the volume removed was determined by measuring the cross-sectional area. Unfortunately, different sample widths caused the force per tooth to change for each experiment. A constant force per cutting tooth was used in the second blade speed experiment and full factorial study by milling samples to precise rectangular dimensions.

In addition to preparing samples of equal width, a finer tooth blade was used in the second speed study. Using a finer tooth blade was motivated by an observation that the Stryker dual-cut blade used in the first study had a tendency to form deep wells in the bone as shown in Figure 11. These wells prevented blade motion, and effectively stopped the sawing process. The switch to a Stryker 2108-210 blade resolved this difficulty.

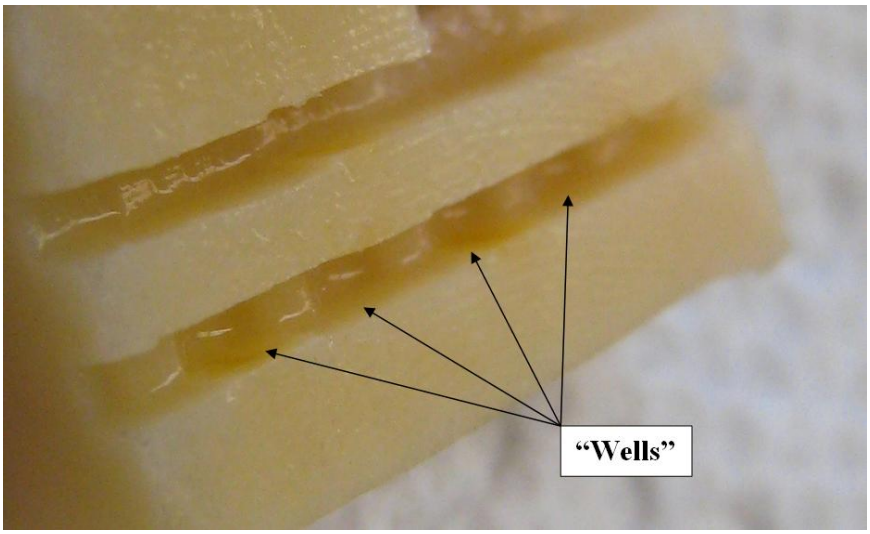

FIGURE 11- Bone "Welling" Behavior

The welling behavior was produced in large part because of the ratio of stroke length to spacing between the teeth. With a large stroke length relative to tooth spacing, several teeth pass over all points on the bone, evenly distributing the cutting loads. If the stroke length is similar to or smaller than the tooth spacing, a high cutting rate is observed at the center of oscillation of each tooth and a lower cutting rate is observed elsewhere. This is because cutting rate is strongly related to blade speed, and in an oscillating saw the blade speed is highest at the center of oscillation. As slight wells are formed beneath the teeth, the stroke length is decreased by deflection in the mechanism as it tries to push the blade out of the wells. Eventually the wells become so deep that the stroke length drops nearly to zero and cutting stops. When this occurred, the motor did not stall, but rather the excess motion was absorbed by deflection in the mechanism.

The primary difference between the blades used in the two speed experiments was their difference in tooth spacing. In the first speed study, the stroke length was slightly smaller than the tooth spacing so the welling behavior was observed. The blade used in the second speed study had a stroke length that was larger than the tooth spacing, which provided for more uniform cutting across the width of the bone. Welling behavior was not observed with this blade.

Another important difference between the blades was that the 2108-210 blade had a slight set to the teeth. A blade is “set” when the teeth are bent slightly out of plane such that the blade is effectively wider at the cutting edge. This reduces friction on the sides of the blade and helps to clear excess chips (3). It was observed that chips were able to “flow” out the top of the cut with the set blade (Stryker 2108-210). In the Dual-Cut blade, the majority of the chips were forced out the edges of the cut. In addition to blade set, the 2108-210 blade had a negative rake angle, where as the Dual-Cut blade had a positive rake angle. The rake angle is the angle between the

cutting face of the tooth, and the normal to the cutting surface. It has been shown that rake angle is important to chip formation (5) (7) (8) (9), and it is possible that this difference affected the welling behavior. The final difference between the blades was that the blade used in the second experiment had a curved end so that all teeth tracked along nearly the same curve during oscillation. The first blade was straight at the end so that the teeth on the edge of the blade traced a slightly different arc than those in the center. Figure 12 shows a photo comparison of each blade, with the Stryker 2108-110 blade on top and the Dual-Cut 4125-135-090 on the bottom. Figure 13 gives a close up comparison of the tooth forms.

FIGURE 12- Photo Comparison of Blades: Stryker 2108-110 (top), Stryker Dual-Cut (bottom)

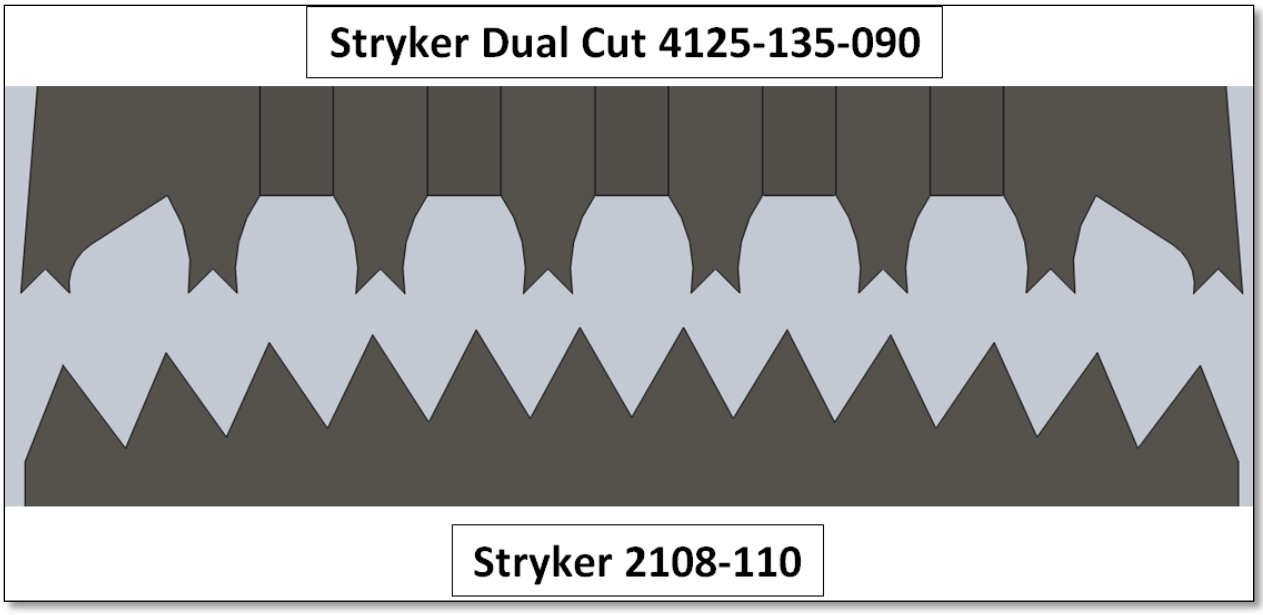

FIGURE 13- Tooth Form Comparison

Data from the second experiment confirmed that cutting rate was strongly related to blade speed, and that there is a critical cutting speed above which the cutting rate increases rapidly. In the second study, the critical blade speed was roughly 650mm/s which was slightly slower than the critical speed observed in the first trial. Additionally, the cutting rates that were observed in the second study varied over a much larger range than in the first study. The differences in critical speed and cutting rates were related to the differences in the experimental parameters, most notable the new blade and larger static load. The results of the second blade speed study are shown in Figure 14, and compared to the first blade speed study in Figure 15.

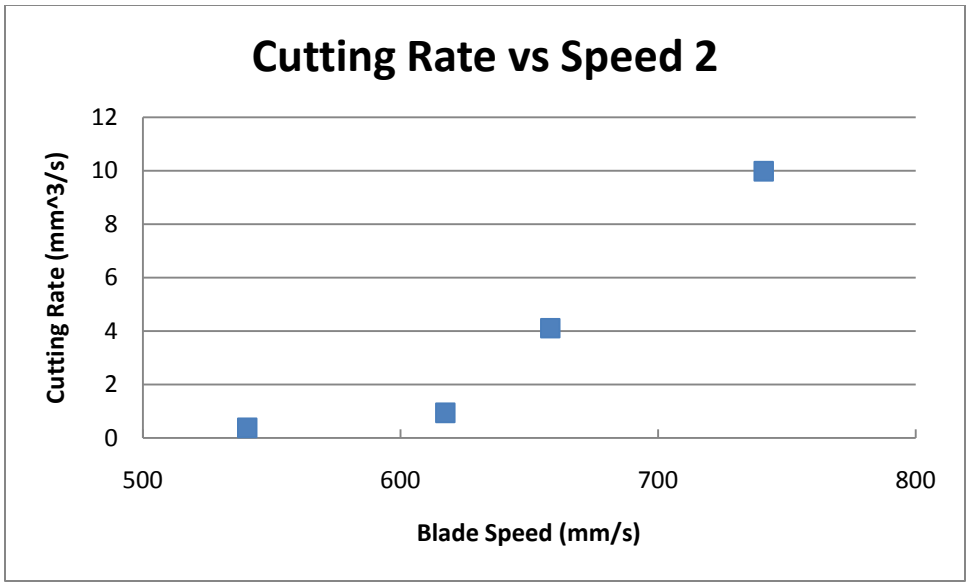

FIGURE 14-Cutting Rate vs. Speed 2

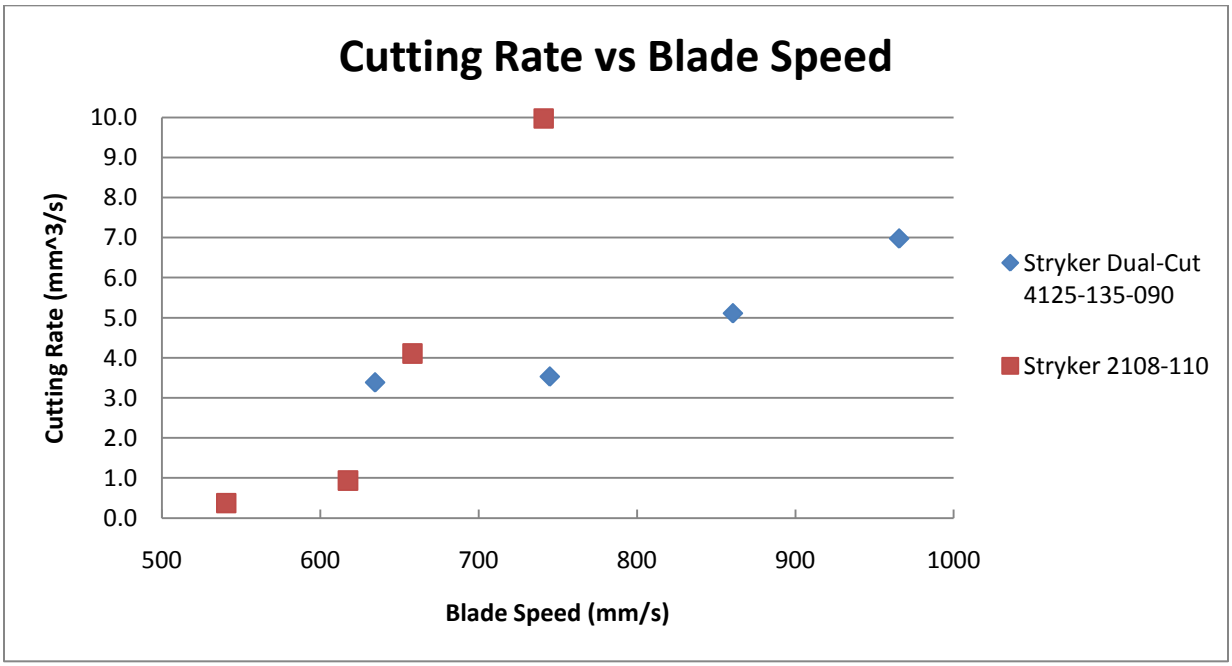

FIGURE 15-Cutting Rate vs. Blade Speed Comparison

It is possible that this critical cutting speed phenomenon is related to the critical cutting speed noted by Krause (8), where the specific energy of the cut decreases above a speed rate of 50mm/s. Although this speed is an order of magnitude lower than those observed in this experiment, it is possible that these differences could be due to the difference in experimental setup. The most significant differences in experimental setup were the range of blade speeds and the DOC. Krause used blade speeds of 1.3-25mm/s and 106-410mm/s, and a DOC of 70um in his trials. The experiments in this thesis were conducted at 500-1000mm/s and theoretical DOC was calculated to be one the order of 1um[2].

Full Factorial Experiment

A final experiment was conducted to examine the effect of static load, blade speed, and thrust amplitude on the cutting rate of bovine bone. This experiment was set up as a three factor, two level, full factorial, design with three measurements at each combination.

Factor Analysis:

There were three factors considered in this experiment: Static Load (A), Thrust Amplitude (B), and Cutting Frequency (C). The effect of each factor and of each combination of factors was calculated and plotted on a Pareto chart (15), as shown in Figure 16. Thrust amplitude had the greatest effect on cutting rate, closely followed by cutting frequency. These results support the hypothesis that impulsive loading, created by the addition of non-zero thrust amplitude, significantly increases cutting rates. The data also shows that cutting rate was dependant on the combination of static load and cutting frequency. This suggests that cutting rate can be improved

[2] As will be discussed later in the section, the actual chips produced by the saw were observed to be roughly an order of magnitude larger than the theoretical value of 1.0um.

by applying a larger static thrust load, but only if it is accompanied by an increase in cutting frequency. Increasing the impulsive thrust force through non-zero thrust amplitude increases the cutting rate regardless of the speed. Therefore, the addition of this motion to a surgical bone saw would have the potential to increase cutting rates.

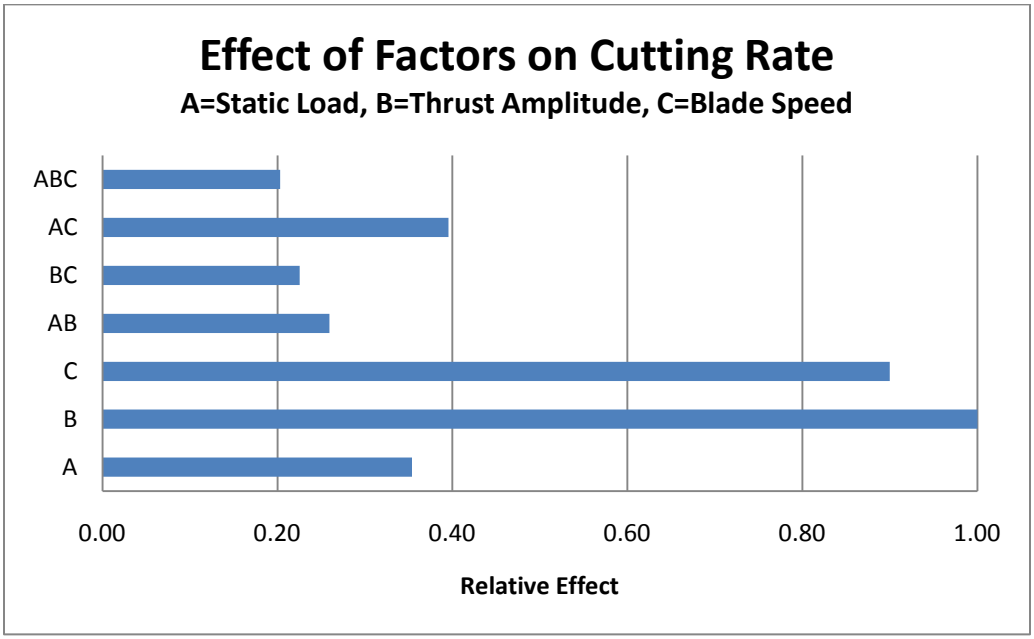

FIGURE 16- Relative Effect of Factors on Cutting Rate

A linear equation can be used to model the data, and shown in Eqn. 5. This equation will return the average experimental values of cutting rate with no residual error. Eqn. 5 can be simplified to the form of Eqn. 6, which takes into account factors and interactions that have the most significant effect on cutting rate. A least squares linear fit of the experimental data was used to determine the coefficients of Eqn. 6. This equation will return values to within 14% of the measured average values.

$\dot{V}$ $Predicted\ Cutting\ Rate\ \left(\frac{mm^3}{s}\right)$

A $Static\ Applied\ Load\ (N)$

B $Thrust\ Amplitude\ (mm)$

C $Blade\ Speed\ \left(\frac{m}{s}\right)$

$$\dot{V} = -5.976 * A + 3472 * B - 71.76 * C - 236.5 * A * B - 5048 * B * C + 8.779 * A * C + 355.9 * A * B * C + 55.52 \qquad Eqn. 5$$

$$\dot{V} \cong -12.9 * A + 158 * B - 223 * C + 19.2 * A * C + 156 \qquad Eqn. 6$$

The addition of non-zero thrust amplitude created an impulsive load on the blade at the start of each cutting stroke. When all other parameters were held constant, the addition of this impulsive force at the start of each cut had the effect of increasing the cutting rate by an average factor of 2.2. Figure 17 shows the difference between trials with and without an impulsive force for each of the four combinations of load and speed. This data verified the hypothesis, showing that a mechanism which creates an impulsive thrust force can be used to create a significant increase in cutting rate.

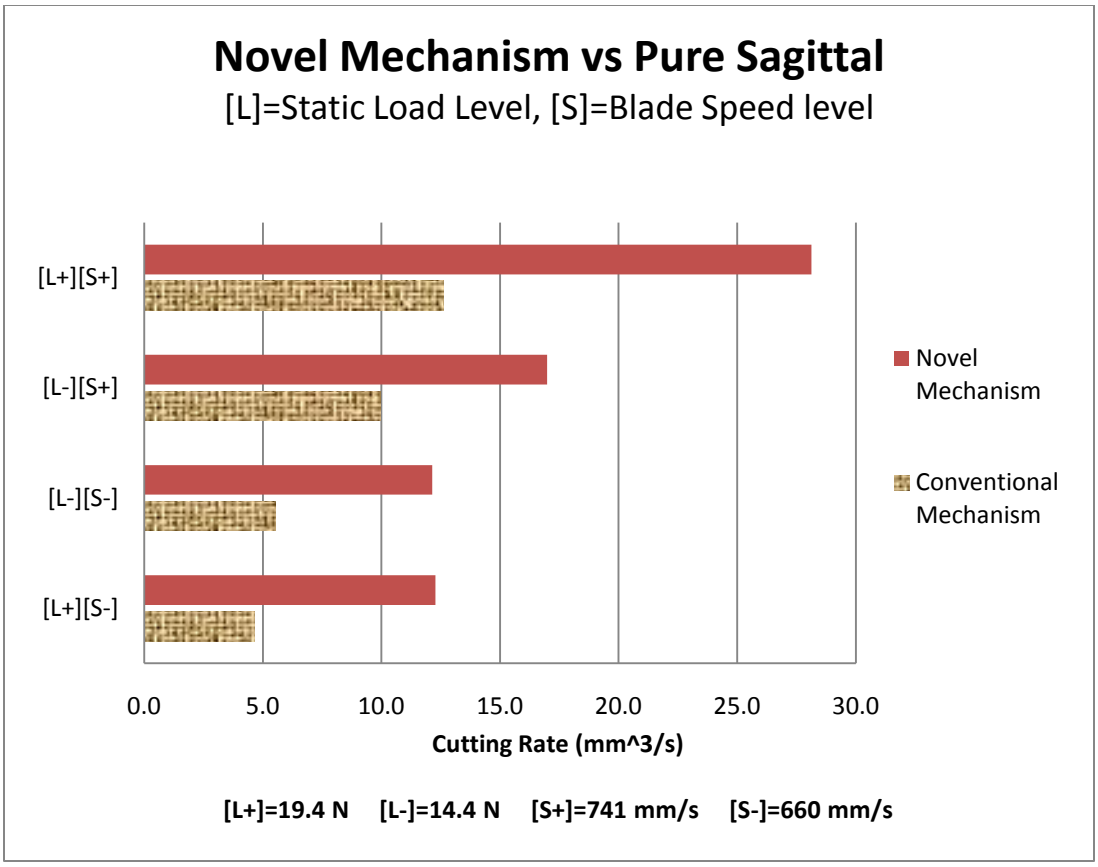

FIGURE 17- Direct Comparison of Orbit Effects

It should be noted that the amplitude of the orbital action in the mechanism was 0.05mm (0.002in), which was on the same scale as the elastic deflection within the mechanism under normal cutting loads. This means that the blade did not necessarily follow a "figure-eight" path when it was cutting. Instead, it was possible that the bone surface altered the path of the blade, and that the difference between ideal and actual path was taken up by the deflection in the mechanism. This deflection would be converted into an additional thrust force by the stiffness of the mechanism, and would distribute the impulse loading over a slightly longer duration. A previous experiment showed that larger thrust amplitude (0.5mm, 0.02in) was not effective at increasing cutting rate because the blade bounced too much to make a clean cut. It is possible that the amplitude must be small enough so that the deflection of the mechanism is enough to adequately distribute the impulsive load to prevent bouncing.

While the addition of an impulsive load increased the cutting rate under all conditions, an increase in static load only increased the cutting rate under specific conditions. For low speeds, the cutting rate was nearly independent of static load within the range considered, as shown in Figures 18 and Figure 19. At higher speeds, an increase in applied load resulted in a more significant increase in cutting rate, particularity in the orbit case.

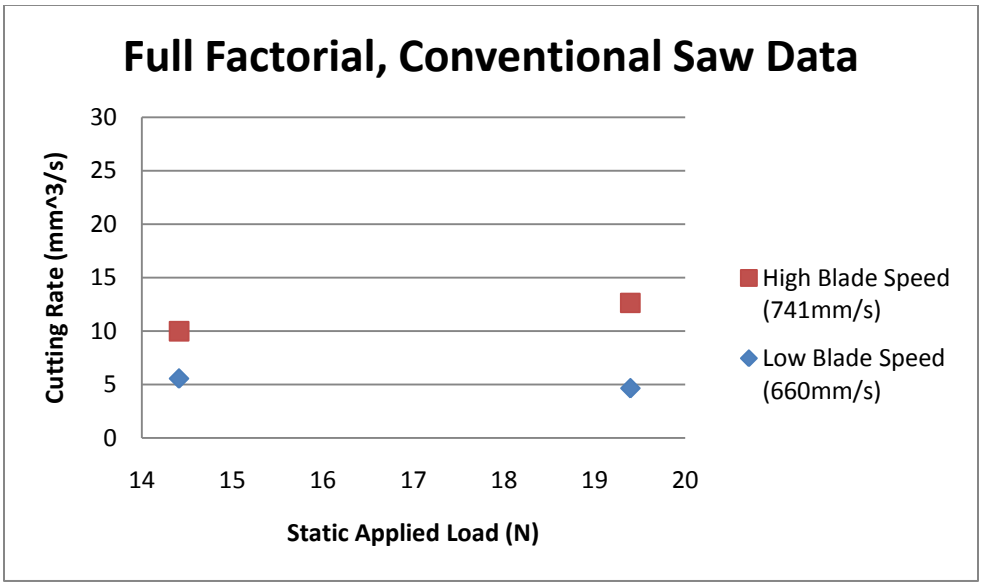

FIGURE 18- Effect of Applied Load for Conventional Saw

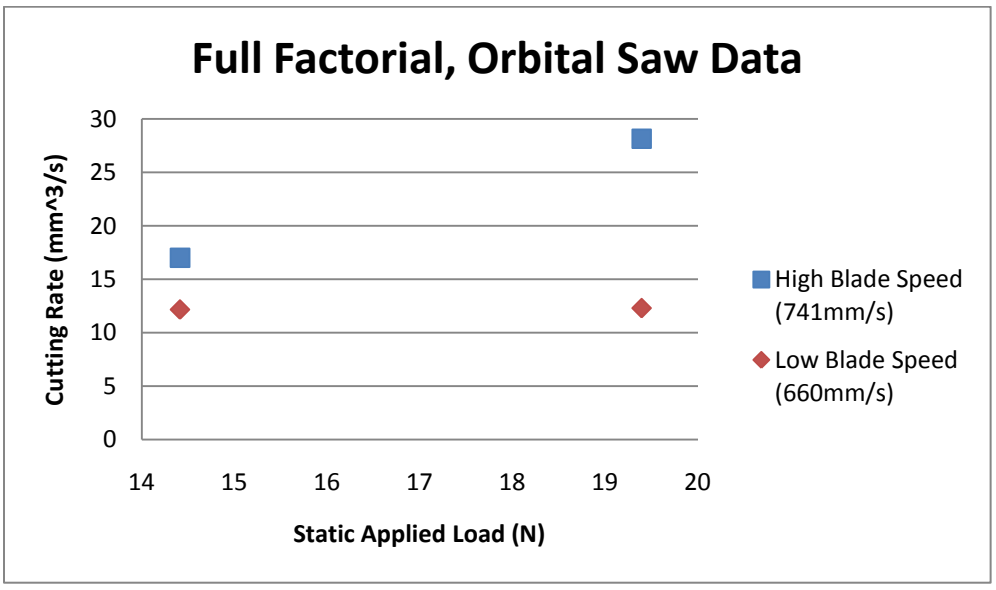

FIGURE 19- Effect of Applied Load for Orbital Mechanism

Depth of Cut Considerations:

Depth of cut is an important metric because it is related to chip formation and the specific energy of cutting. In the majority of studies, the DOC is a controlled experimental parameter. In these experiments however, the DOC was allowed to be a dependent variable. This arrangement is similar to what would be observed during surgery. The average theoretical DOC can be calculated based on a few assumptions as shown in Eqn. 7-12. Based on these equations, the average theoretical DOC per tooth was calculated to be on the order of 1.0um (0.04mil).

V_c $volume\ per\ chip$
L $length\ of\ a\ cutting\ stroke$
w $kerf\ width$
δ $chip\ thickness\ (DOC)$
N_c $chips\ formed\ per\ stroke$
B $bone\ sample\ width$
p $saw\ tooth\ spacing$
V_t $total\ volume\ removed$
H $bone\ sample\ height$
N $number\ of\ chips\ formed$
f $cutting\ frequency$
t $duration\ of\ cut$

First, assume that chips are formed as rectangular prisms with the full width of the kerf, the length of the cutting stroke, and of a uniform thickness to be determined.

$$Volume\ per\ chip: V_c = L * w * \delta \qquad Eqn.\ 7$$

Next, assume that on every stroke all blade teeth form a chip. Allow for a fractional number to account for the chips near the edge of the bone that are not formed to the full stroke length. The number of chips formed per stroke is the number of teeth that are engaged.

$$Chips\ per\ stroke: N_c = B/p \qquad Eqn.8$$

The total volume of bone removed is assumed to be a rectangular prism with the full width of the kerf and the cross sectional area of the bone sample.

$$Total\ volume: V_t = B * w * H \qquad Eqn.9$$

Assume that chips are formed evenly in both cutting directions, uniformly across duration of cut, and at a constant cutting frequency.

$$Number\ strokes: N = 2 * f * t \qquad Eqn.10$$

Determine the total volume of chips produced by multiplying volume per chip, chips per stroke, and number of strokes. Assume that this volume is equal to the total volume removed.

$$Total\ Chip\ Volume: \sum V_c = (L * w * \delta) * \left(\frac{B}{p}\right) * (2 * f * t) = V_t = B * w * H \qquad Eqn.11$$

Solving Eqn. 11 for chip thickness, δ, and simplifying:

$$\delta = \frac{H * p}{2 * f * t * L} \qquad Eqn.12$$

Figure 20 shows a correlation between the theoretical DOC and cutting rate. It can be shown that the slope of this linear relation is a function of several constant experimental parameters and the average cutting frequency across all trials.

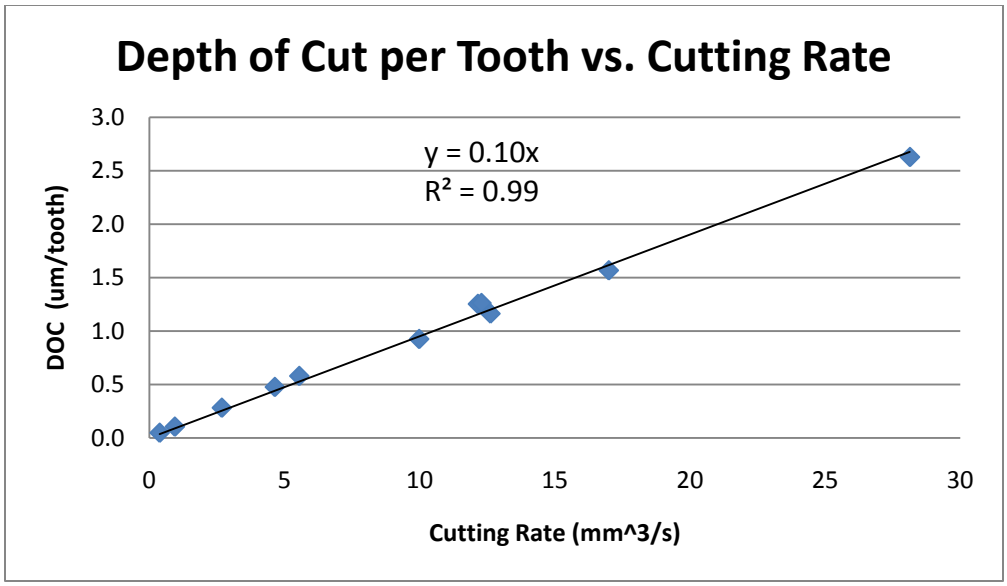

FIGURE 20- Depth of Cut per Tooth vs. Cutting Rate

Figure 20 shows a linear relationship between average theoretical DOC and cutting rate, suggesting that mechanisms that increase the theoretical DOC will increase the cutting rate. Although the theoretical DOC is predicted to be on the order of 1-2um, the chips that were produced were observed to be roughly an order of magnitude larger than this. It is possible that chips are not formed by every tooth on every blade stroke. If this were the case, then the theoretical DOC would predict a smaller DOC than was observed, according to Eq. 13. For example, if a tooth passes a given point ten times before creating a chip, then the chip that is produced would be ten times the thickness predicted by Eqn. 12.

$\overline{DOC}$ $Average\ Theoretical\ DOC$
n $Number\ of\ teeth\ that\ pass\ a\ given\ point\ in\ the\ bone$
DOC_i $Actual\ DOC\ (often = 0)$
D $Average\ Real\ DOC\ when\ a\ chip\ is\ formed$
N $Number\ of\ teeth\ that\ pass\ before\ chip\ is\ formed$
P $Probability\ that\ a\ chip\ will\ be\ formed\ of\ size\ D$

$$\overline{DOC} = \frac{1}{n}\sum_{i=0}^{n} DOC_i \cong \frac{D}{N} = D * P \qquad Eqn.\,13$$

Figure 20 shows that an increase in the theoretical DOC is likely to produce an increase in cutting rate. Eqn. 13 predicts that the theoretical DOC and therefore cutting rate could be increased through two possible methods. The first method would be to increase the size of chips that are removed, and the second would be to increase the probability that a chip will be created. An impulsive thrust force, like that used in the experiment, would likely increase DOC through one or both of these modes. This can be shown by determining the factors that are critical to theoretical DOC. Figure 20 shows a chart of the relative effect on DOC of the three experimental factors, and thrust amplitude is the strongest factor. This suggests that creation of an impulsive thrust loading is an effective method of increasing the cutting rate because it increases the theoretical DOC.

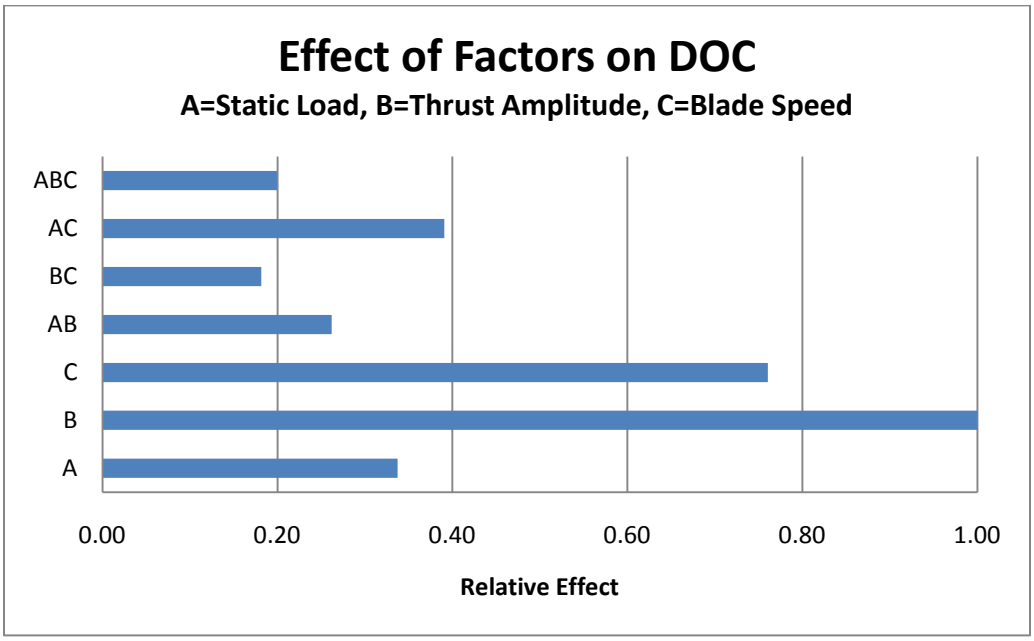

FIGURE 21- Factors Relevant to Depth of Cut

Process Outliers:

During some of the trials, the saw was observed to cut through a portion of the bone at a constant rate, stop for a period of several seconds, and then continue at the original rate. At the time of these experiments the data was recorded with a note describing the behavior. In later experiments, which were outside the scope of this thesis, a similar behavior was observed. In these experiments, this behavior was related to errors in the experimental process rather than an effect of the bone sawing process. For this reason, these experimental cutting rates were neglected in considering the data. In some trials, this reduced the number of data points such that a standard deviation was no longer a valid description of the data, and thus error bars were not included on the plots. Appendix C provides the complete data sets for the experiments, including the outliers, which are noted as such.

6 Conclusions

Three experiments were performed, two of which explored the effect of blade speed on the cutting rate in bovine bone. The third experiment was a three factor, two level, full factorial experiment on cutting rate. The factors considered were static load, thrust amplitude and blade speed.

The results of the experiments confirmed the hypothesis that an impulsive thrust force applied during bone sawing increases the cutting rate. In general, the mechanism used in this experiment roughly doubled the cutting rate when compared to the conventional sagittal bone saw under otherwise identical conditions.

It was determined that thrust amplitude was the strongest factor in determining cutting rate. The figure-eight blade path imparted an impulsive thrust load on the bone surface. It was proposed that an impulsive thrust load increased cutting rate by forming larger chips. The thrust amplitude was 0.05mm (0.002in), which was at the lower tolerance limit of the mechanism. Future mechanisms may be simplified by replacing the gear set and off-center crank with an electromechanical or pneumatic device.

All experiments showed that cutting rate was dependent on blade speed. There was a critical speed above which the cutting rate significantly increased. The critical blade speed was determined to be 650-800 mm/s for the parameters used in this study. This finding suggests that previous studies (5) (8) which were carried out at low cutting speeds of 1-25mm/s may not accurately reflect the nature of bone sawing.

It was previously thought that the static thrust load would be a critical factor in determining cutting rate. It was found that increasing the static thrust load only increased the cutting rate for speeds well above the critical blade speed.

Several calculations were made regarding the average depth of cut per tooth which was found to be on the order of 1.0um. It was noted that there is a possibility that chips are not formed by every tooth on every cutting stroke. This would explain why the theoretical depth of cut was smaller than the observed bone fragment size. Additionally, it is proposed that impulsive loading and high blade speeds result in large cutting rates because they increase the probability that a chip will be produced, or that they increase the size of the chip produced. Orthogonal machining analysis assumes that a single tooth cutting at a constant depth of cut is representative of the entire saw blade. The findings of this experiment suggest that this not necessarily an accurate assumption.

7 Future Work

The experiments indicate that the modified blade path increased cutting rate. However, the number of trials was small, and some data points were neglected as outliers. Additional experiments are required to support the validity of ignoring outliers, as well as providing information as to the statistical significance of the results.

It was shown that cutting rate is a nonlinear function of blade speed. There was a critical speed, above which the cutting rate increased significantly. Future work could explore the cause of this critical speed, and its dependence on applied load. A more thorough understanding of this phenomenon could also be used to instruct surgeons on the proper amount of load to apply to a saw for each blade speed that is used during surgery.

High and low blade speeds were used in the design of experiments. It was shown that the relationship between cutting rate and blade speed was nonlinear. A more accurate model would be obtained by a three or four level study.

The depth of cut considerations in this experiment showed that chips are not necessarily being formed by every tooth that passes across the bone surface. This makes it difficult to calculate the chip formation mechanisms from the cutting rate and sample data. A microscopic analysis of the bone fragments formed by the sawing process could lead to a better understanding of the chip formation process. This could then be used to develop a better understanding of why the incorporation of the impulsive thrust loading improved the cutting rate.

Finally, modern bone saws show deficiency in both cutting rate and heat produced during cutting. The work of this thesis addresses only the cutting rate of the novel sawing mechanism. Further studies could investigate the heat generated by this saw to determine if an orbital blade path could be used to reduce the cutting temperatures observed in surgery.

8 Works Cited

1. *Influence of Irrigation Solutions on Oscillating Bone Saw Blade Performance.* **Timmon W. Ark, Jeffrey G. Neal, John G.Thacker, Richard F. Edllich.** s.l. : John Wiley & Sons, Inc, 1998.

2. *A New Mechanistic Approach for Micro End Milling Force Modeling.* **Martin B.G. Jun, Chanseo Goo, Mohommad Malekian, Simon S. Park.** Vancouver, British Columbia, Canada : ASME International ME Congress & Exposition, 2010.

3. *Orthopedic Sawblades, A case study.* **H.W.Wevers, E.Espin, T.D.V.Cooke.** 1, s.l. : The Journal of Arthroplasty, 1987, Vol. 2.

4. *Effects of Tourniquet During Total Knee Arthroplasty.* **Anwar Abdel-Salam, Keith S. Eyres.** s.l. : The British Editorial Society of Bone and Joint Surgery, 1995, The Journal of Bone and Joint Surgery, Vols. 77-B:250-3.

5. *Orthogonal Machining of Bone.* **K. L. Wigging, S. Malkin.** s.l. : Journal of Biomechanical Engineering, 1978, Vol. 100, pp. 122-130.

6. *Specifications for Machining the Bovine Cortical Bone in Relation to its Microstructure.* **Naohiko Sugita, Mamoru Mitsuishi.** s.l. : Journal of Biomechanics, 2009, Vol. 42, pp. 2826-2829.

7. *Modelling and Optimization of Bone-Cutting forces in Orthopaedic Surgery.* **Christopher Plaskos, Antony J. Hodgson, and Philippe Cinquin.** s.l. : Springer-Verlag Berlin Heidelberg, 2003.

8. *Orthogonal Bone Cutting: Saw Design and Operating Characteristics.* **W.R.Krause.** s.l. : ASME, 1987, Journal of Biomechanical Engineering.

9. *Basic Study on Bone Cutting Forces for developing Surgical Instruments.* **Shuzo Itoh, Yoshimi Ito.** 222, s.l. : Bulletin of JSME, 1983, Vol. 26.

10. *"Chip Formation, friction, and High Quality Machined Surfaces".* **Ernst, H., and Merchant, M. E.** s.l. : ASM, 1941, Surface Treatment of Metals.

11. *"Basic Mechanics of the Metal Cutting Process".* **Merchant, M. E.** s.l. : ASME, 1944, Journal of Applied Mechanics, Vol. 11, pp. A168-A175.

12. **Papworth, W. A.** Manually Portable Power Driven Cutting Tool with Oval Stroke. *US Patent 2,917,088.* Dec. 15, 1959.

13. **Richard E. Walton, II, Fallston, Md.** Orbital Jig Saw. [ed.] Black & Decker Inc. *US Patent No. 4,238,884.* Dec. 16, 1980.

14. **Thomas Richard Bednar, Roger Dean Neitzell, Michael Scott Steele.** Orbital Recprocating Saw. [ed.] Milwaukee Electric Tool Corperation. *US Patent No. 6,249979.* Jun. 26, 2001.

15. **Barrentine, Larry B.** *An Introduction to Design of Experiments.* s.l. : American Society for Quality, 1999.

9 Appendix

Appendix A: Blade Path Analysis

The path that the tip of the saw blade follows is based on the geometry of the components shown in Figure A. Several parts have been removed so that the internal workings of the mechanism are visible. The off-center axis for each crank shaft is constrained to the center plane of the corresponding linear guide through bearings which are not shown.

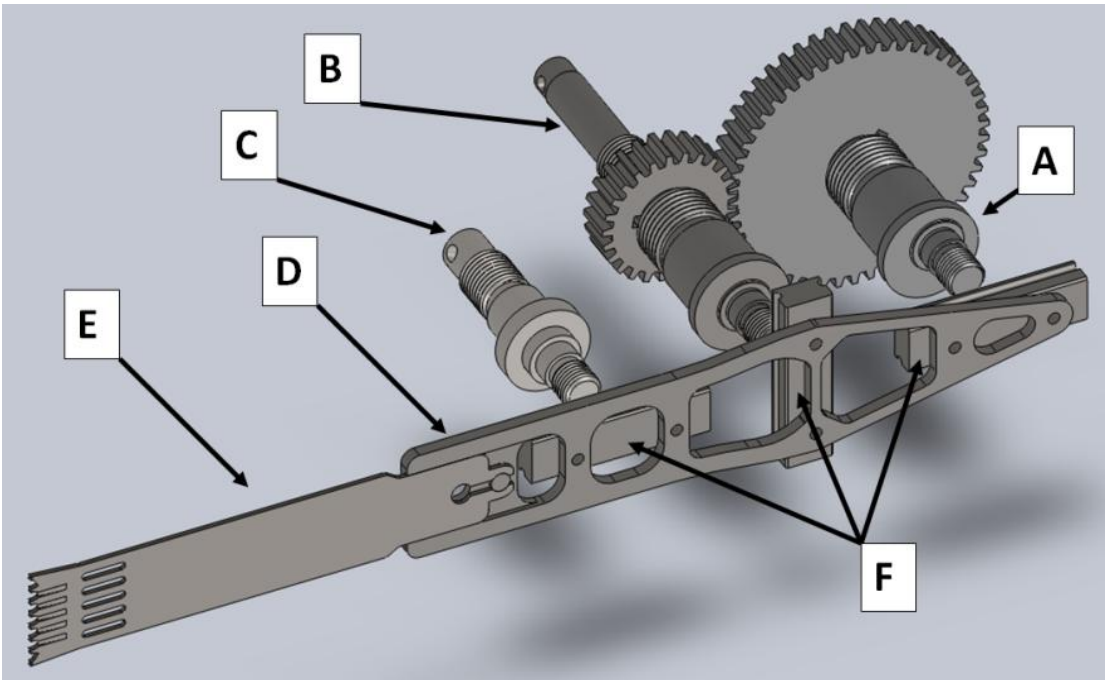

Appendix Figure A- Novel Sawing Mechanism Key Components

Shaft angles θ and φ are related through gearing with a constant gearing offset angle γ. Angle θ is associated with crankshaft A, and angle ϕ is associated with crankshaft B. Eqn. A1 gives the relation between these three angles.

$$\theta = -\frac{1}{2}\varphi + \gamma \qquad Eqn.A1$$

Each off-center crankshaft drives its crank in a circle. Eqn. A2, Eqn. A3, and Eqn.A4 give the location of the center of each crank as a function of time. P1 is the center of shaft C, P2 is the center of the off-center crank on shaft B, and P3 is the center of the off-center crank on shaft A.

δ: $Radial\ Offset\ of\ \ Crankshaft\ A$
ε: $Radial\ Offset\ of\ Crankshaft\ B$
L_A: $Spacing\ between\ shafts\ B\ and\ C$
L_B: $Spacing\ between\ shafts\ A\ and\ B$

$$P_1 = \langle 0,0 \rangle \qquad Eqn.\ A2$$

$$P_2 = \langle L_A + \varepsilon \cos\theta\, , \varepsilon \sin\theta \rangle \qquad Eqn.\ A3$$

$$P_3 = \langle L_A + L_B + \delta \cos\varphi\, , \delta \sin\varphi \rangle \qquad Eqn.\ A4$$

Apply constraints created by linear guides (Eqn. A5). Define a reference frame $\boldsymbol{a}$ which is attached to the blade base (D), with orthogonal components $\boldsymbol{a_1}$ and $\boldsymbol{a_2}$. $\boldsymbol{a_1}$is collinear with linear bearings (F) on shafts A and C, directed to the right. $\boldsymbol{a_2}$ is collinear with linear bearing (F) on shaft B, directed up.

$$a_2 \cdot (P_3 - P_1) = a_{2x}P_{3x} + a_{2y}P_{3y} = 0 \qquad Eqn.\ A5$$

The next section shows how to express the unit vector $\boldsymbol{a}$ in terms of known parameters. The subscripts x and y are used to denote the orthogonal components of the vector a in the inertial, stationary, reference frame. When the blade is centered, the x ordinate is directed along the length of the blade and the y ordinate is directed normal to the length of the blade. The magnitude of a unit vector is 1, and the orthogonal components are related by Eqn. A6.

$$|a| = \sqrt{{a_x}^2 + {a_y}^2} = 1 \qquad Eqn.\,A6$$

Vector a_2 is normal to vector P_3 by definition, thus their dot product must be zero.

Algebraic manipulation of the dot product yields Eqn. 7.

$$\frac{a_{2x}}{a_{2y}} = \frac{-P_{3y}}{P_{3x}} \qquad Eqn.\,A7$$

Algebraic manipulation of Eqn. A6 yields Eqn. A8.

$$a_{2y} = \left[1 - \left(\frac{a_{2x}}{a_{2y}}\right)^2\right]^{-\frac{1}{2}} \qquad Eqn.\,A8$$

Substituting Eqn. A7 into Eqn. A8 yields Eqn. A9.

$$a_{2y} = \left[1 - \left(\frac{-P_{3y}}{P_{3x}}\right)^2\right]^{-\frac{1}{2}} \qquad Eqn.\,A9$$

Rearranging Eqn. A7 yields Eqn. A10.

$$a_{2x} = a_{2y}\left(\frac{-P_{3y}}{P_{3x}}\right) \qquad Eqn.\,A10$$

Eqns. A11-A12 are based on the definition of an orthogonal coordinate system.

$$a_{1y} = -a_{2x} \qquad Eqn.\,A11$$

$$a_{1x} = a_{2y} \qquad Eqn.\,A12$$

Define a point Po to be along the blade. With respect to the origin, this point can be defined by traveling a distance along the length axis of the blade, and then a distance from the center plane along the edge of the blade with teeth. The distance r is the distance from the center plane for the point under consideration. The path of the center tooth of the blade is found by setting r=0.

Express Po as function of known vectors:

$$P_0 = (P_2 \cdot a_1 - L)a_1 + (r)a_2 \qquad Eqn.A12$$

Plot using MatLab:

```
% This script will plot the path of three teeth on the blade for
% various phase angles. Each tooth path is displayed on its own
% graph. The teeth used in this case are the center, and 2mm to
% each side.

for i=0:23
    phase_D=mod(i,8)*180/8;           %phase offset in degrees
    phase=phase_D*pi/180;             %Convert to Radians
    Tooth_Space=2;                    %mm
    r=-(floor(i/8)-1)*Tooth_Space     %Tooth location
    theta=linspace(0,2*pi,100);
    phi=2*(phase-theta);

    La=47.6;                          %mm
    Lb=47.6;                          %mm
    L=198.4;                          %mm
    d=0.1524;                         %mm
    e=1.7526;                         %mm

    P2x=La+d.*cos(phi);
    P2y=d.*sin(phi);
    P3x=La+Lb+e.*cos(theta);
    P3y=e*cos(theta);

    A2y=(1-(-P3y./P3x).^2).^-0.5;
    A2x=A2y.*(-P3y./P3x);
    A1x=A2y;
    A1y=-A2x;
    d=P2x.*A1x+P2y.*A1y;
```

```
    Pox=A1x.*(d-L)+r*A2x;
    Poy=A1y.*(d-L)+r*A2y;
    subplot(3,8,i+1); plot(Pox+150.8,Poy);
    axis([-0.25 0.25 -5 5]);
    xlabel('Thrust Direction (mm)')
    ylabel('Cutting Direction (mm)')
    if i<8
        title(['Phase Offset: ' num2str(phase_D) ' (deg)'])
    end
end
```

In the following diagrams, A, B, and C are the traces of a point on the blade. A and C are defined for points that are 2mm from the center plane of the blade, and are symmetric to each other. Point B is the center of the blade. These points do not necessarily correspond to a particular tooth, depending on the tooth spacing of the blade being considered. Figures C and D show the blade path for a variety of gearing phase offsets and for tooth positions A, B, and C.

Appendix Figure B- Blade Path Tooth Locations

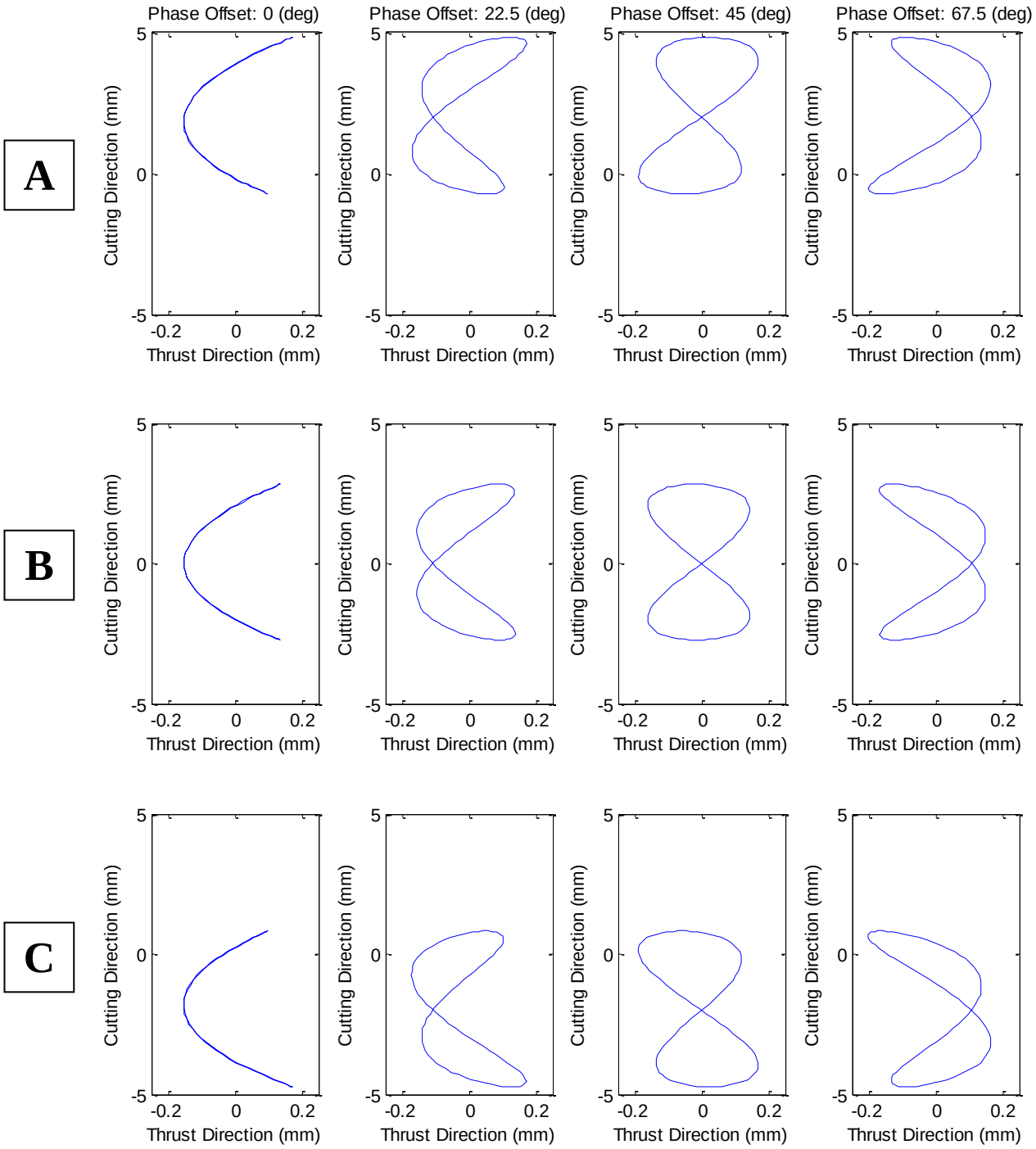

Appendix Figure C-Blade Paths for Gearing Phase Less Than 90°

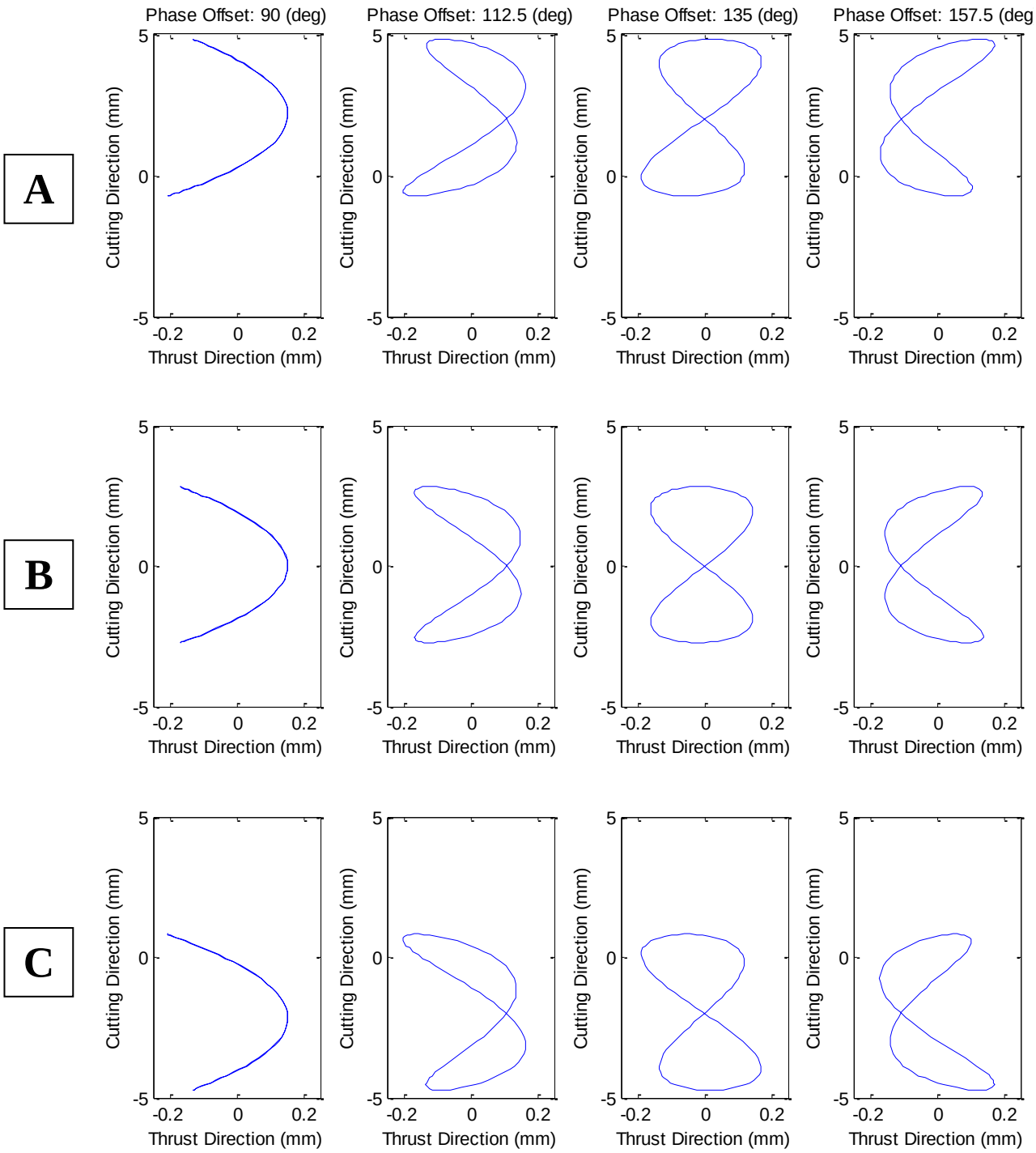

Appendix Figure D-Blade Paths for Gearing Phase Greater Than 90°

Appendix B: Fixture Force Analysis

When the saw cuts through a bone sample, the fixture rotates. This rotation causes a slight variation in the constant force applied by the fixture.

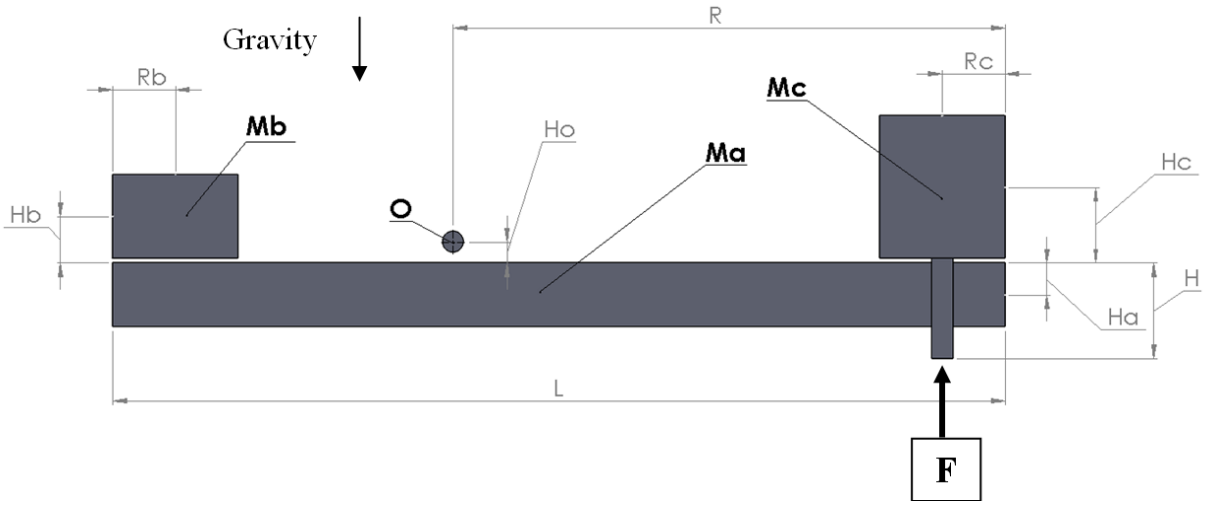

Appendix Figure E-Model for Determining Deviations from Static Load

Define the inertial coordinate system located at point O on Figure E.

$$\begin{aligned} &\mathrm{x} = \text{ordinate directed to the right, normal to gravity} \\ &\mathrm{y} = \text{ordinate directed up, antiparallel to gravity} \\ &\langle \mathrm{x}, \mathrm{y} \rangle = \text{Inertial coordinate system notation} \end{aligned}$$

Let positive θ be measured counterclockwise from the positive x axis. Define the rotational reference frame i and j by the following unit vectors and centered at point O.

$$\begin{aligned} &i = \langle cos(\theta)\,, sin(\theta) \rangle \\ &j = \langle -sin(\theta), cos(\theta) \rangle \\ &\{i, j\} = Rotational\ reference\ frame\ coordinate\ system \\ &Example\colon \{A, B\} = \langle Acos(\theta) - Bsin(\theta), Asin(\theta) + Bcos(\theta) \rangle \end{aligned}$$

Define points corresponding to the center of mass of the three primary components in the rotational coordinate system.

$$P_A: \quad \left\{R - \frac{1}{2}L\,, -(H_o + H_A)\right\}$$
$$P_B: \quad \{R_B - (L - R)\,, H_B - H_o\}$$
$$P_C: \quad \{R - R_C\,, H_C - H_o\}$$
$$P_F: \quad \{R - R_C\,, -(H_o + H)\}$$

Transform points to inertial coordinate system:

$$P_A: \quad \langle (R - 0.5 * L)\, cos(\theta) + (H_o + H_A)\, sin(\theta)\,, (\, R - 0.5 * L)\, sin(\theta) - (H_o + H_A)\, cos(\theta)\rangle$$
$$P_B: \quad \langle \big(R_B - (L - R)\big)\, cos(\theta) - (H_B - H_o)\, sin(\theta)\,, \big(R_B - (L - R)\big)\, sin(\theta) + (H_B - H_o)\, cos(\theta)\rangle$$
$$P_C: \quad \langle (R - R_C\,)\, cos(\theta) - (H_C - H_o)\, sin(\theta)\,, (R - R_C\,)\, sin(\theta) + (H_C - H_o)\, cos(\theta)\rangle$$
$$P_F: \quad \langle (R - R_C)\, sin(\theta) + (H_o + H)\, cos(\theta)\,, (R - R_C)\, cos(\theta) - (H_o + H)\, sin(\theta)\rangle$$

Assuming that the fixture is stationary, Eqn. A13 provides an equation for the sum of moments (T) created by each of the three massive bodies and reaction force F about point O.

$$\sum T_o = T_A + T_B + T_C + T_F = 0 \qquad Eqn.\,A13$$

Eqn. A14 expresses the sum of the moments in terms of force (W or F) multiplied by the corresponding lever arm (P).

$$P_A * W_A + P_B * W_B + P_C * W_C = -P_F * F \quad ; \quad * = \ cross\ product \qquad Eqn.\,A14$$

The weight vectors are directed parallel to gravity, and gravity is assumed to be constant. The force F is assumed to be directed along the length of the blade, in the thrust direction when the blade is at the center of its path. Eqns. A15 and A16 follow from these assumptions.

$$W_i = M_i\langle 0, -g\rangle \qquad Eqn.\,A15$$

$$F = F\{0,1\} = F\langle -sin(\theta)\,, cos\ (\theta)\rangle \qquad Eqn.\,A16$$

Evaluate cross products yields Eqn. A17.

$$
\begin{aligned}
-g\big(M_A[(R-0.5*L)\,cos(\theta)+(H_o+H_A)\,sin(\theta)] \\
&+M_B\big[\big(R_B-(L-R)\big)\,cos(\theta)-(H_B-H_o)\,sin(\theta)\big] \\
&+M_c[(R-R_C)\,cos(\theta)-(H_C-H_o)\,sin(\theta)]\big) \\
&=F(cos(\theta)[(R-R_C)\,cos(\theta)-(H_o+H)\,sin(\theta)] \\
&+sin(\theta)[(R-R_C)\,sin(\theta)+(H_o+H)\,cos(\theta)]) \qquad Eqn.A17
\end{aligned}
$$

Solving for F yields equation A18.

$$
\begin{aligned}
F=&\frac{-g\cdot cos(\theta)\left(M_A(R-0.5*L)+M_B\big(R_B-(L-R)\big)+M_c(R-R_C)\right)}{(H_o+H)[sin(\theta)\,cos(\theta)-sin(\theta)\,cos(\theta)]+(R-R_C)[sin(\theta)^2+cos(\theta)^2]} \\
&+\frac{-g\cdot sin(\theta)\big(M_A(H_o+H_A)-M_B(H_B-H_o)-M_c(H_C-H_o)\big)}{(H_o+H)[0]+(R-R_C)[1]} \qquad Eqn.A18
\end{aligned}
$$

Simplify and collect terms to find Eqn. A19.

$$
\begin{aligned}
F=&\left(\frac{-g}{R-R_c}\right)\{[M_a(R-0.5*L)+M_b(R_b-L+R)+M_c(R-R_c)]Cos(\theta) \\
&+[M_a(H_0-H_a)+M_b(H_0-H_b)+M_c(H_0-H_c)]Sin(\theta)\} \qquad Eqn.A19
\end{aligned}
$$

Matlab was used to plot the force variation across the range of angles which were observed during the experiments. Plots were created for three separate nominal static loadings, and shown in Figure F. The values of the various parameters that were used can be found in the following Matlab code.

```
function Tipper_Force

% Determine how blade tip force and tipper angle are related
% Dynamics calculations page 3

% set constants:
Ma=8.30;         %mass of rails (kg)
Mb=22.16;        %mass of countermass (kg)
Mc=11.47;        %mass of saw asembly (kg)
g=9.81;          %gravity (m/s^2)
Ha=0.038;        %height of COM for tipper rails (m)
Hb=0.038;        %height of countermass COM (m)
Hc=0.080;        %height for saw COM (m)
H0=0.025;        %height of main tipper axle (m)
H=0.114;         %height for blade tip (m)
L=1.067;         %total length of tipper rails (m)
Rb=0.076;        %distance from rail end to countermass COM (m)
Rc=0.075;        %distance from rail end to saw COM (m)

Convert_To_Rad=pi/180;
Theta_Max=.35*Convert_To_Rad;    %Upper bound for angle (degrees)
Theta_min=-.35*Convert_To_Rad;   %Lower bound for angle (degees)
Theta=linspace(Theta_min,Theta_Max,500);        %Create array of angles

R=[0.65 0.66 0.67];     %distance from main axle to saw end of rail (m)
Arc_Distance_1=sqrt((R(1)-Rc)^2+H^2)*Theta_Max-Theta_min
Arc_Distance_2=sqrt((R(2)-Rc)^2+H^2)*Theta_Max-Theta_min
Arc_Distance_3=sqrt((R(3)-Rc)^2+H^2)*Theta_Max-Theta_min

F_1=(g/(R(1)-Rc))*(cos(Theta)*(Ma*(R(1)-0.5*L)+Mb*(Rb-L+R(1))+Mc*(R(1)-Rc))-
      sin(Theta)*(Ma*(H0+Ha)+Mb*(H0-Hb)+Mc*(H0-Hc)));
F_2=(g/(R(2)-Rc))*(cos(Theta)*(Ma*(R(2)-0.5*L)+Mb*(Rb-L+R(2))+Mc*(R(2)-Rc))-
      sin(Theta)*(Ma*(H0+Ha)+Mb*(H0-Hb)+Mc*(H0-Hc)));
F_3=(g/(R(3)-Rc))*(cos(Theta)*(Ma*(R(3)-0.5*L)+Mb*(Rb-L+R(3))+Mc*(R(3)-Rc))-
      sin(Theta)*(Ma*(H0+Ha)+Mb*(H0-Hb)+Mc*(H0-Hc)));

subplot(3,1,1) , plot(Theta/Convert_To_Rad,F_1);
xlabel('Angle (degrees)')
ylabel('Applied Thrust Load (Newtons)')
title('Load versus Angle, Radius 0.65m')

subplot(3,1,2) , plot(Theta/Convert_To_Rad,F_2);
xlabel('Angle (degrees)')
ylabel('Applied Thrust Load (Newtons)')
title('Load versus Angle, Radius 0.66m')

subplot(3,1,3) , plot(Theta/Convert_To_Rad,F_3);
xlabel('Angle (degrees)')
ylabel('Applied Thrust Load (Newtons)')
title('Load versus Angle, Radius 0.67m')
```

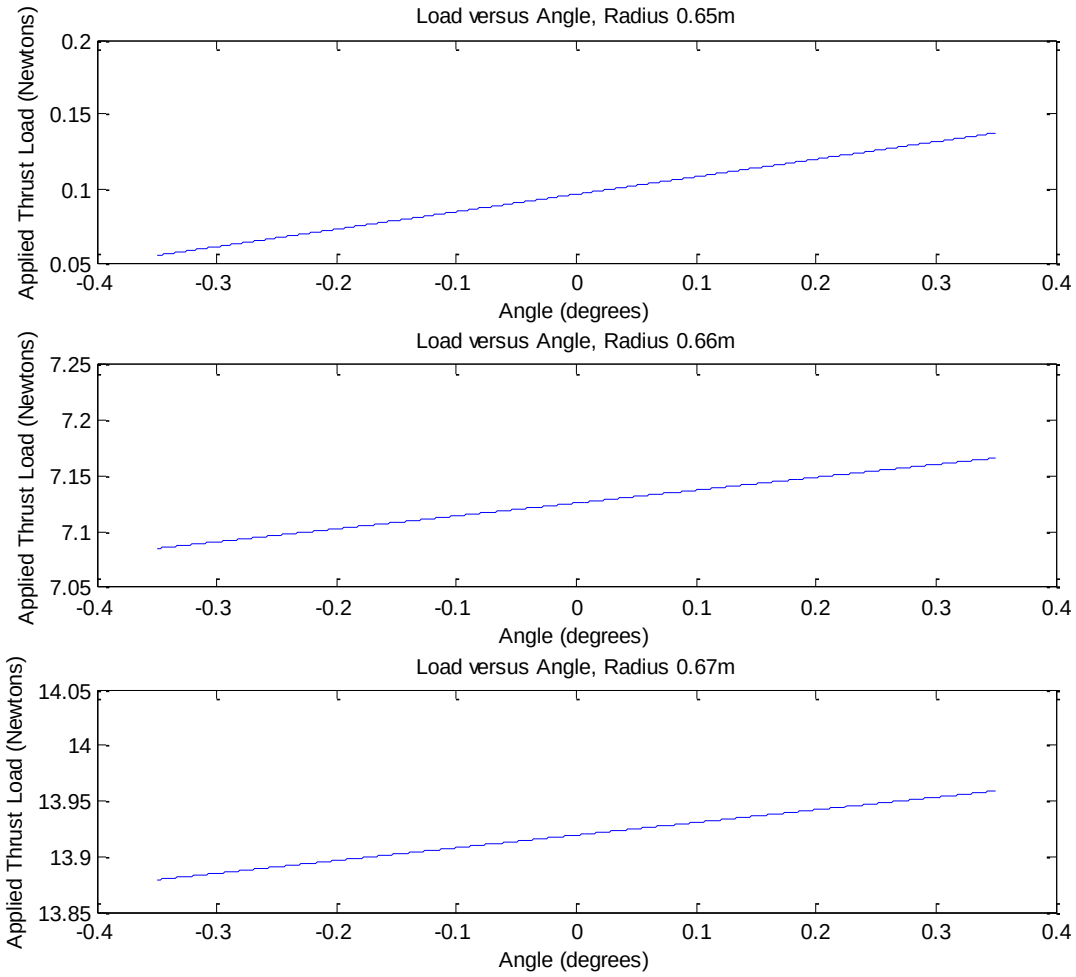

Appendix Figure F- Calculated Deviations from Static Load

Appendix C: Experimental Data

Appendix C contains the raw data collected for all experiments.

Blade Speed Study 1: Data from Trials 25-36. The kerf width measured in this trial was 1.19mm (0.047in) and the applied load was 7.6N (1.7lbf).

Blade Speed Study 2: Data from Trials A-C, 1-6

Full Factorial Study: Data from Trials 1-24

Trial Number	A	B	C	1	2	3	4	5	6
Load (N)	14.4			14.4			14.4		
Load (lbf)	3.24			3.24			3.24		
Thrust Amplitude (um)	0			0			0		
Thrust Amplitude (mil)	0			0			0		
Speed (kRPM)	14.0	16.0	17.0	17.1			19.2		
Cut Freq (Hz)	117	133	142	143			160		
Avg Speed (mm/s)	541	617	656	660			741		
Width (mm)	19.5	19.5	19.5	19.2	19.8	19.9	19.3	19.6	20.1
Height (mm)	6.0	6.0	6.0	5.8	5.5	5.2	5.8	5.5	5.3
Vol. Rm. (mm^3)	187	187	187	178	174	166	179	172	170
Sample Density (kg/m^3)	2091	2091	2091	1934	2027	2312	1934	2027	2312
Mass (g)	0.39	0.39	0.39	0.34	0.35	0.38	0.35	0.35	0.39
Sample Number	NA	NA	NA	1	2	3	1	2	3
Time (s)	500	200	70	23.9	29.1	52.1	16	17.5	19.2
Vol. Rate (mm^3/s)	0.37	0.94	2.67	7.46	5.99	3.18	11.19	9.86	8.88
Mass Rate (mg/s)	0.78	1.96	5.59	14.42	12.14	7.35	21.65	19.98	20.52
DOC (um)	0.05	0.10	0.28	0.79	0.62	0.33	1.06	0.92	0.80
Process Outlier	NO			NO			NO		
Avg Cut. Rate (mm^3/s)	0.4	0.9	2.7	5.5			10.0		

Appendix Figure G- Experiential Data for Trials A-C, 1-6

Trial Number	7	8	9	10	11	12	13	14	15
Load (N)	19.4			19.4			14.4		
Load (lbf)	4.36			4.36			3.24		
Thrust Amplitude (um)	0			0			50.8		
Thrust Amplitude (mil)	0			0			2		
Speed (kRPM)	17.1			19.2			17.1		
Cut Freq (Hz)	142.5			160			142.5		
Avg Speed (mm/s)	660			741			670.8		
Width (mm)	21.7	19.6	19.9	19.6	19.7	20	19.8	19.7	19.9
Height (mm)	5.6	5.6	5.3	5.9	5.8	5.4	5.5	5.7	5.6
Vol. Rm. (mm^3)	194	176	169	185	183	173	174	180	178
Sample Density (kg/m^3)	2091	2027	2312	1934	2027	2312	1934	2027	2312
Mass (g)	0.4066	0.356	0.3902	0.3578	0.3706	0.3995	0.337	0.3642	0.4122
Sample Number	123	2	3	1	2	3	1	2	3
Time (s)	139	65.2	36.4	14.5	12.8	16	15.9	18	11.5
Vol. Rate (mm^3/s)	1.3988	2.6935	4.636	12.76	14.283	10.8	10.958	9.9813	15.505
Mass Rate (mg/s)	2.9249	5.4597	10.719	24.678	28.951	24.97	21.194	20.232	35.847
DOC (um)	0.13	0.28	0.48	1.19	1.32	0.98	1.13	1.04	1.59
Process Outlier	YES		NO	NO			NO		
Avg Cut. Rate (mm^3/s)	4.6			12.6			12.1		

Appendix Figure H- Experiential Data for Trials 7-15

Trial Number	16	17	18	19	20	21	22	23	24
Load (N)	14.41			19.39			19.39		
Load (lbf)	3.24			4.36			4.36		
Thrust Amplitude (um)	50.80			50.80			50.80		
Thrust Amplitude (mil)	2.00			2.00			2.00		
Speed (kRPM)	19.2			17.1			19.2		
Cut Freq (Hz)	160.0			142.5			160.0		
Avg Speed (mm/s)	753.1			670.8			753.1		
Width (mm)	19.7	19.7	19.8	19.7	19.8	19.9	19.4	19.6	19.9
Height (mm)	5.4	5.6	5.5	5.6	5.6	5.4	5.4	5.5	5.5
Vol. Rm. (mm^3)	170	177	174	177	177	172	169	172	175
Sample Density (kg/m^3)	1934	2027	2312	1934	2027	2312	1934	2027	2312
Mass (g)	0.33	0.36	0.40	0.34	0.36	0.40	0.33	0.35	0.40
Sample Number	1.0	2.0	3.0	1.0	2.0	3.0	1.0	2.0	3.0
Time (s)	12.20	10.50	8.62	86.00	73.30	14.00	5.71	6.46	23.80
Vol. Rate (mm^3/s)	13.95	16.81	20.21	2.05	2.42	12.28	29.57	26.70	7.36
Mass Rate (mg/s)	26.98	34.08	46.73	3.97	4.91	28.39	57.19	54.12	17.01
DOC (um)	1.29	1.55	1.86	0.21	0.25	1.26	2.78	2.48	0.67
Process Outlier	NO			YES		NO	NO		YES
Avg Cut. Rate (mm^3/s)	17.0			12.3			28.1		

Appendix Figure I- Experiential Data for Trials 16-24

Trial Number	Router Speed (RPM)	Speed (Hz)	Time to cut (s)	Area (mm^2)	Volumetric Cutting Rate (mm^3/s)	Average Cutting Rate (mm^3/s)	Standard Deviation
25	11500	95.8	24.34	73.2	3.59	3.39	0.19
26			29.84	84.1	3.36		
27			25.63	68.9	3.21		
28	13500	112.5	30.37	91.9	3.61	3.53	0.15
29			29.68	90.1	3.62		
30			38.44	108.3	3.37		
31	15500	129.2	29.78	108.4	4.35	5.11	0.71
32			23.38	102.3	5.22		
33			20.00	96.5	5.76		
34	17500	145.8	13.31	69.4	6.23	6.97	0.67
35			11.28	71.1	7.53		
36			12.06	72.4	7.17		

Appendix Figure J- Experiential Data for Trials 25-36